Materials for Quantum Technology

OPEN ACCESS

RECEIVED
24 February 2025

REVISED
17 May 2025

ACCEPTED FOR PUBLICATION
23 June 2025

PUBLISHED
3 July 2025

TOPICAL REVIEW

A review of site-controlled compound semiconductor quantum dots for single photon emitters

Yaonan Hou

Electronic and electrical engineering, Swansea University, Bay Campus, SA1 8EN Swansea, United Kingdom
Centre for Integrative Semiconductor Materials (CISM), Swansea University, Bay Campus, SA1 8EN Swansea, United Kingdom

E-mail: yaonan.hou@swansea.ac.uk

Keywords: semiconductor, quantum dot, site control, scalability, coherence

Abstract

Single photon emitters (SPEs) serve as the fundamental building blocks of photonic networks for applications in quantum information science and technology. This review paper focuses specifically on the rapidly growing area of site-controlled and deterministically fabricated compound semiconductor quantum dots (QDs), which holds great potential for scalability given their high quantum efficiency, flexible coherence tunability and compatibility with silicon photonics. In this paper, the state-of-the-art growth and fabrication approaches, integration with photonic structures have been reviewed. Meanwhile, the emission properties from QD-based SPEs, including brightness, purity and coherence tunability, have been discussed. This review also provides an outlook of future developments of site-controlled QDs, offering insights into the progress toward scalable quantum photonic systems.

1. Introduction

1.1. Overview of single photon emitters (SPEs)

The fast development of low-loss optical systems, especially the COMS-compatible Si photonics, enables manipulating photonic quantum bits (Q-bits) on a chip for quantum information processing, with examples including but not limited to quantum computing [1, 2], quantum key distributions [3], quantum sensing and simulating [4, 5]. The advancement of processing quantum information at the system level proves the scalability of photonic quantum building blocks with a low cost, compared with the approaches in superconducting circuits, trapped ions/atoms, and spintronics [6–8]. It is also the driving force of the requirement for on-chip and scalable quantum light sources-SPEs, which emit one photon at a time. Such devices can also be applied in super-resolution imaging, single molecular sensing, high-precision metrology, secure biometric identification and so on. However, the SPEs adopted in quantum photonic systems so far still primarily rely on spontaneous parameter down conversion (SPDC) and attenuating a laser light down to single photons, which is bulky and not integrable, associated with problematic statistics in single photon emission probability (purity) and low quantum efficiency (defined as the ratio of number of emission photons over the number of excitation photons or electrons) [9]. In contrast, the advancement in semiconductor quantum dots (QDs), especially the development of high-brightness compound QDs with site-controlled growth and deterministic fabrication, well aligns with the Si photonics for on-chip integration. Therefore, this review will focus on the recent progress in site-controlled compound QDs and their pathway to scalable quantum photonic systems.

Before moving to the next section, it is worth summarising and comparing the state-of-the-art SPEs, including their working principles, advantages and challenges. This will be helpful in selecting the appropriate quantum source for a designated quantum network. An overview of different types of SPEs is shown in figure 1, with their working mechanism and properties summarised as below.

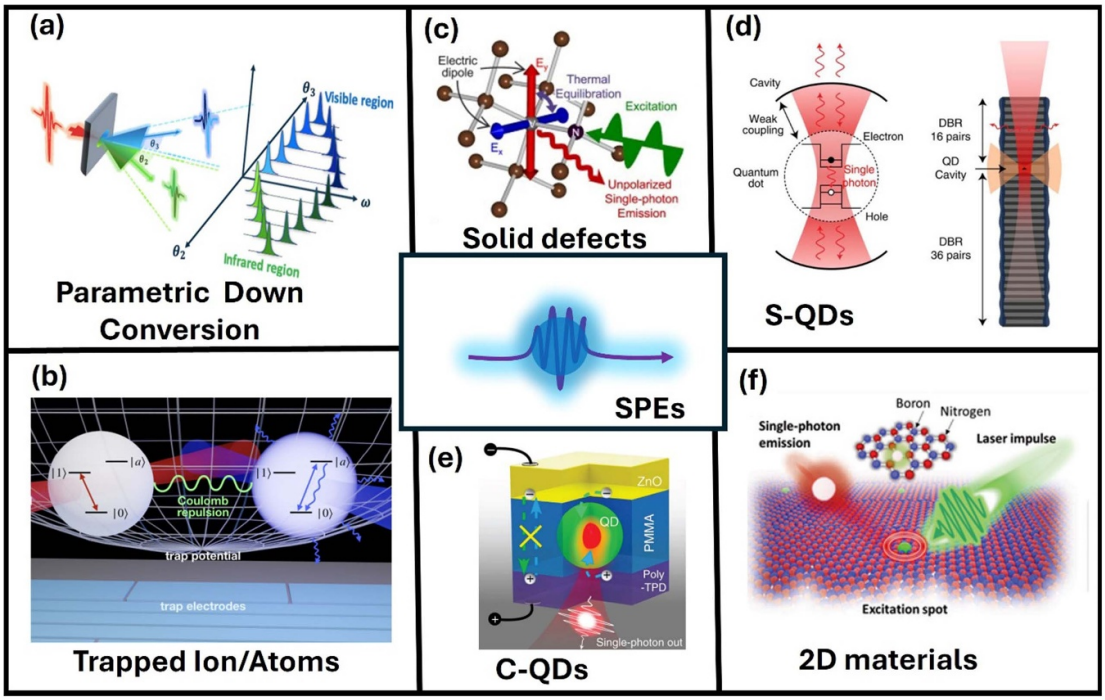

Figure 1. An overview of the single photon emitters. (a) Photon pairs generated by spontaneous parametric down-conversion; Reproduced from [10]. CC BY 4.0. (b) Schematic of trapped ions/atoms manipulated with light; Reproduced from [14], with permission from Springer Nature. (c) NV centres in diamond; Reproduced from [15]. CC BY 4.0. (d) InAs quantum dot coupled with a DBR cavity by epitaxial growth; Reproduced from [25], with permission from Springer Nature. (e) Electrically pumped colloidal quantum dot for single photon emission; Reproduced from [28]. CC BY 4.0. (f) Single photon emission from 2D materials, Reproduced from [32]. CC BY 4.0.

- **SPDC** utilises nonlinear crystals (such as BBO, $LiNbO_3$, BBLN etc) to down-convert high-frequency laser into two longer-wavelength beams/pulses, namely signal and idler, by means of three- or four-wave mixing (schematically shown in figure 1(a)) [10]. The process requires phase-match conditions, which ensures energy and momentum conservation. SPEs based on SPDC can generate heralded single photons (photon pairs with highly correlated states) and entangled states because they inherit the optical properties from the coherent laser source [11]. Due to this, SPDC are predominantly used by quantum startups, e.g. PsiQuantum, ORCA computing, QuiX quantum and so on. However, there are apparent drawbacks, including (1) the purity of the source is low, where >1 or 0 photons may be generated under external excitation. (2) Quantum efficiency and brightness are low, limited by the nature of the process. (3) Requirement of stringent phase match conditions, i.e. delicate positioning of the nonlinear crystal. (4) Relying on the external laser hinders the on-chip integration.
- **Single atom/ion/molecular** contains at least two discrete energy levels, a ground state $|g\rangle$ and excited state $|e\rangle$. Under external excitation, a single photon will be emitted when the electron transit from $|e\rangle$ to $|g\rangle$. The typical materials used for such SPEs include Rb and Cs atoms; Ca^+, Yb^+, Sr^+, Ba^+ ions; and Terrylene, PAHs, DBATT molecules [12, 13]. As the energy levels of the materials are highly discrete and electron spin status can be controlled with an external magnetic/electric field, the coherence (e.g. same energy, polarisation, phase) of the photons is high, with the capability of operating at room temperature. The single atom/ion often needs an optical or electromagnetic trap to localise them and isolate them from the perturbations (schematically shown in figure 1(b)) [14], whilst the single molecule requires host materials and suffers from photon bleaching. Both scenarios pose challenges for scaling them up to a quantum system.
- **Colour centre** is a point defect in solids, which has similar energy levels as that of a single atom/ion. Typical materials are the nitrogen-vacancy centres (NV) and Si vacancy (Si-V) in diamond (schematically shown in figure 1(c)) [15, 16], and point defects or defect pairs in wide bandgap semiconductors such as SiC, ZnO, GaN, AlN and so on [17–20]. The unique electronic structure offers a narrow emission spectrum (so-called zero phonon line, or ZPL). Therefore, colour centres are high-purity SPEs, with the demonstration working at room temperature [21]. Since the host materials are mostly direct bandgap, electrically pumped single-photon emission is significantly promising [22]. One disadvantage of the colour centre is that such defects are often randomly located in their host, a significant challenge for scalability. A recent breakthrough demonstrates that periodic colour centres (G- and W-centres) in silicon can be fabricated using a focused

ion beam (FIB) [23]. However, this technique is not compatible with mass production. The other drawback is that the colour centre could couple to its surroundings (e.g. another adjacent defect) [24], leading to decoherence.

- **Semiconductor QDs (S-QDs)** refer to atomic-like, solid-state semiconductor clusters synthesised by epitaxial growth in this review. Such 'artificial atoms' have energy levels that resemble the Rydberg energy of an isolated atom, $E(n) \propto -\frac{R}{n^2}$ (where $E(n)$ is the exciton energy, R is a constant relevant to the material, n is the quantum number). QDs are often described as two-level systems (i.e. $n \sim 2$), given the quantum confinement effects arising from their finite size in a cladding layer. Due to the fast development of semiconductor manufacturing, there are several advantages recognised for S-QD SPEs: (1) near unity internal quantum efficiency of the direct band gap semiconductor materials, (2) high brightness as the carrier lifetime can be engineered down to picosecond level with Purcell effect (examples in figure 1(d)) [25], (3) the spatial mode can be tailored to satisfy the demand, (4) high-purity and high-indistinguishability photons have been achieved from single S-QDs, essential for a quantum system, (5) the fabrication process, including QD growth or post-growth processing, is well established in semiconductor community [26, 27]. (6) The mature semiconductor photonic integrated system (e.g. fast-speed Si optical transceivers have been widely deployed in datacentres) positions S-QD as a significant promising candidate for on-chip quantum information processing. The challenges for S-QDs include their random distribution on a wafer for scalability and the coherence of photons emitted from different QDs. But both the challenges are not unsolvable based on the recent progress, to be reviewed in this paper.
- **Colloidal QDs (C-QDs)** share the same working mechanism as that of S-QDs, but they are synthesised by solution-based methods normally with a core-shell structure (e.g. figure 1(e)) [28]. Therefore, C-QDs are cost-effective compared with S-QDs. Although the primary applications of C-QDs are in displays and lighting, recent progress demonstrates single C-QDs are competent working as SPEs, even under electrical injection [28]. Limited by the synthesis method, C-QDs normally contain surface defects and residual ligands [29], which require passivation to increase the quantum efficiency and brightness [30]. Moreover, the uniformity of morphology (e.g. size and shape) results in coherence issues for photons emitted by different C-QDs. The major challenge of C-QDs is the difficulty of fabricating site-controlled coherent SPEs by the liquid-based approaches, which is incompatible with the established CMOS semiconductor processing techniques.
- **2D materials** are emerging quantum materials for high-performance SPEs. Typical 2D-QDs are formed by introducing lateral confinement using small patches or creating a confined electrical field by accommodating local strain (figure 1(f)) [31, 32]. It is worth mentioning that the latter approach has been successfully applied to create site-controlled SPE arrays, opening a route to scalability [33]. Besides, defects in 2D materials are also candidates for SPEs [34]. Benefiting from the broad diversity of 2D materials (e.g. h-BN, graphene, transition metal dichalcogenides, MXenes and 2D oxides) [35], various unique 2D SPEs have been developed, e.g. working under room temperature and/or electrically pumping [33]. As 2D materials are sensitive to their environment (e.g. substrates, surface adsorbates, defects etc), emission light from 2D QDs often has a low quantum yield and inhomogeneous broadening. The other challenge is how to scale up the 2D-QD array with a high photon extraction efficiency and prescribed coherence.

Table 1 shows a summary of the diverse SPEs employing different techniques. Each of them is developing dynamically, with advantages and drawbacks compared with another. Therefore, it is challenging to determine which is superior or to identify a definitive ultimate solution for scalability. In light of this, the summary above aims to provide a concise overview of the SPEs and their features, serving as a tutorial for the readers. Hopefully, the information can be helpful for them to select suitable candidates for their photonic quantum systems or address the related challenges. For a detailed overview of recent advancements in each type of SPE, please refer to the respective review papers and the references therein [11, 12, 30, 31, 36, 37].

Despite significant efforts and advancements in quantum materials, this review paper will focus on *site-controlled* compound semiconductor QD-based SPEs, particularly because of their promising potential for compact quantum systems by integrating with the rapidly growing Si photonic building blocks (i.e. waveguiding devices). Instead of discussing the quantum physics of the S-QD SPEs, this review aims to offer an engineering perspective, including fabrication approaches and key characteristics, towards an integrated quantum photonic system.

1.2. State-of-the-art of S-QDs: concept, growth, fabrication, integration and site-control

To provide a clear visual example, figure 2(b) displays the morphology of epitaxial InAs QDs observed by (AFM and X-STM) [38, 39]. As shown in the example, the S-QDs are usually a comparatively narrower band gap semiconductor (e.g. InAs) epitaxially grown in a wider bandgap gap host semiconductor material (e.g. InP and GaAs). The formation of S-QDs is driven by the surface energy and the local strain, leading to

Table 1. Overview of the SPEs with the fabrication approaches and their characteristics.

SPEs	Fabrication methods	Advantages	Challenges
SPDC	• Nonlinear crystal with laser pumping	• High coherence • Entangled photon pair generation • Deployed in quantum photonic startups	• Bulky and incompatible with on-chip integration • Low quantum efficiency • Low purity
Single Atom/ Ion/Molecular	• Atom/Ion traps with laser excitations • Hosting materials	• High coherence • Room temperature working	• Bulky and require external traps or hosting materials
Colour centres	• Ion implantation • Doping • Annealing	• High coherence • Room temperature working	• Random distribution
Colloidal QDs	• Solution based process	• Easy fabrication	• Surface defects/ligands (non recombination centres) • Low coherence between dots
Semiconductor QDs	• Epitaxial growth • Top-down fabrication	• Site-controlled fabrication availability • High quantum efficiency • Convenience in optical engineering • Promising in on-chip salability (photonic integration) • Compatible with industrial semiconductor manufacturing • Potential in electrical pumping	• Coherence between dots requires further development • On-chip integration still at a preliminary stage
2D materials	• Exfoliating • Epitaxial growth and deposition • Electroplating	• Various fabrication options • Site-controlled fabrication availability • Convenience in optical engineering	• Optical property vulnerable to the environment • Low coherence between emitters • Solution for scalability not clear yet

growth dynamics following the Stranski–Krastanov growth mode (i.e. a 3D island growth dynamics). The shape and the size could be modulated by growth parameters (e.g. temperature, pressure, doping) to realise the quantum confinement and delta-like density of states.

As stated above, the S-QDs are often treated as a two-level system due to the quantum confinement. The electron-hole pairs in the S-QDs will be combined as a quasi-particle, known as an exciton. The energy levels of an exciton are depicted in figure 2(a) (left), where the degenerated level emits photons with an energy of,

$$h\nu_{\mathrm{H,V}} = E_{\mathrm{g}} - E_X$$

where H, V are the emitted photons with polarisations determined by the electron states without considering the spin state, E_{g} ground and excited stage energy difference (bandgap), and E_X the electron–hole binding energy. The degenerated excited state can be split into different levels considering the two spin states. With changing the electronic environment of the exciton (e.g. photonic structure, magnetic field etc) [44, 45], it is possible to select one of the polarised emitting photons to enhance the coherence. In the case of bi-exciton, a three-level (or higher) system can be established, as shown in the right of figure 2(a). Due to the intermedium single exciton states, two-photon emission can be expected. The total emission energy will be,

$$\sum h\nu_{H,or\,V} = E_g - E_{XX}$$

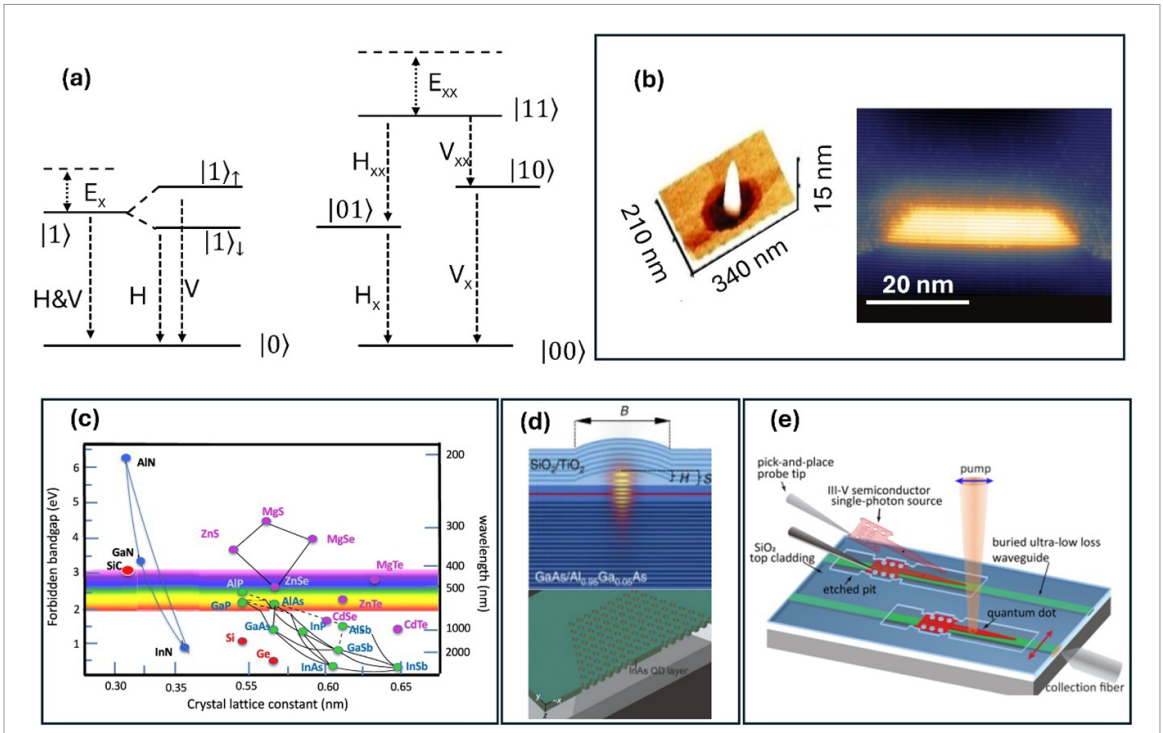

Figure 2. (a) Schematic of the energy levels of an exciton (left) and a bi-exciton (right) in QDs. (b) Morphology of III–V QDs measured by AFM and X-TEM; AFM image. Reproduced from [38]. CC BY 4.0. [39] John Wiley & Sons. © 2020 WILEY-VCH Verlag GmbH & Co. KGaA, Weinheim. (c) Bandgap map of major semiconductors, Reproduced from [40]. CC BY 4.0. (d) III–V QDs coupled with a DBR cavity (top) and a PhC cavity (bottom); Reproduced from [41]. CC BY 4.0. Reproduced from [42], with permission from Springer Nature. (e) Schematic of hybrid integration of III–V QD single photon emitter with an ultra-low loss SiN waveguide by pick-and-place method, Reproduced from [43]. CC BY 4.0.

where the E_{XX} is the bi-exciton binding energy. The process of bi-exciton emission is useful to create entangled photon pairs [46], similar to down-converted photon pairs but with a much better quantum efficiency.

There is a vast solid-state semiconductor material family for the fabrication of S-QDs, with emission wavelengths ranging from UV to mid-infrared. Figure 2(c) shows the bandgap gap energy as a function of the lattice constant of semiconductors [40]. As one can see, the stable light-emitting materials are dominated by group III–V compounds. For example, the UV–visible wavelength range is dominated by the III-nitride group, whilst the near-infrared light is mainly III-As or III-P groups. Typical mid-infrared materials are the InAs or InSb and their alloys. It is worth noting that II–IV materials (e.g. ZnS, CdS, CdSe etc) offer additional QD platforms for emitting UV–visible light. They are more present as solution-processed C-QDs than in the form of epitaxial S-QDs [30].

To demonstrate a few advantages of mature post-growth device fabrication of S-QDs, figure 2(d) displays a few examples. In the top panel, a single S-QD based on GaAs is fabricated inside an open cavity fabricated by distributed Bragg reflectors (DBRs). Due to the overlap between the cavity mode and emission spectrum of the S-QD, the brightness can be enhanced 40 folds with an improved near-unity quantum efficiency and a purity of $g^2(0) = 0.044$, through a strong Purcell effect [41]. Moreover, the strong coupling between the photon's electromagnetic field and the S-QD's dipole can generate bosonic quasiparticles such as polaritons, opening a way to investigate novel quantum physics in light-matter interactions [47], exampled with Bose–Einstein condensates, ultralow threshold polariton lasers, quantum superfluidity and so on [48–50]. Besides the 3D structures, the S-QD can also be fabricated into a 2D slab photonic crystal (PC) cavity/waveguide, which offers a strong optical confinement [27, 42]. Moreover, the engineered photonic structure will guide the single photons into designated optical modes, improving indistinguishability/coherence. Recent reports demonstrated pure $|H\rangle$ (or $|V\rangle$) emission can be selected by coupling an S-QD with a metasurface comprising concentric gratings, significantly improving the coherence and brightness [44, 51]. In the meantime, the progress in electrically injected S-QD SPEs working at room temperature poses a promising potential for on-chip quantum sources [52, 53].

Photonic integration by post-growth fabrication is the key pathway towards on-chip scalable photonic quantum systems. The technique requires interconnecting multiple QDs with the photonic components developed in Si photonics, typically waveguide and waveguiding devices [54]. There have not been many

breakthroughs so far in this area; related publications will be discussed in detail in section 3 of this review. Before this, it will be helpful to have a foundational understanding of the approaches and challenges in photonic integrations of Si photonics with compound semiconductors. In Si photonics, photonic integration methods can be categorised into three regimes: hybrid integration, heterogeneous integration and monolithic integration, with details outlined below [55, 56].

Hybrid integration indicates the interconnection of two or more photonic dies (chips) at the packaging stage. For example, coupling a prefabricated QD-based SPE with a silicon photonic chip using flip-chip bonding or pick-and-place transferring. The advantage of this method is simple, cost-effective and allows pre-selection of the components with desired optical properties. However, there are also obvious challenges to overcome due to the involvement of mechanical alignment, including (1) the optical loss between the two photonic chips (insertion loss) is often high, reduces the brightness; (2) the yield of the integrated platform is low; (3) the integration density is low, not suitable for large scale quantum photonic networks.

Heterogeneous integration includes compound semiconductor QD materials transferring onto Si (e.g. by wafer bonding or transfer printing), which facilitates the subsequent fabrication of SPEs, Si photonic components and interconnectors. Compared with hybrid integration, this method is promising for low insertion loss between SPEs and waveguides, with higher yield and integration density. However, the optical properties of QDs are likely to change due to the materials transfer and bonding, which may introduce strain, defects and cracks.

Monolithic integration refers to epitaxial growth of compound semiconductor QDs on Si, with the subsequent device fabrication at its minimum footprint and seamless integration on the same wafer. As the post-growth fabrication is CMOS-compatible, this method is suitable for manufacturing quantum photonic systems at the wafer level with ultra-high integration density and a compromised cost. However, its challenge lies in high-performance semiconductor QD epitaxial growth due to the material property differences between compounds and Si (e.g. lattice constant difference and thermal expansion coefficient difference).

For waveguide-coupled QD-SPEs, only hybrid and heterogeneous integration approaches have been adopted so far, while monolithic integration has not been reported. As a recent example, Chanana *et.al* demonstrated S-QD based SEPs integration with ultra-low loss waveguides (~ 1 dB m^{-1}), where high purity of $g^2(0) = 0.04 \pm 0.02$ under resonant excitation (figure 2(e)) [43], essential for scaling up S-QD to quantum systems.

Although ultra-low loss waveguiding devices, such as ring resonators, multiplexers, modulators and so on, have been well established, the integration of multiple QDs on the same photonic chip is still at a preliminary stage [57]. This can be attributed to two main reasons. For the first, most of the epitaxially grown QDs are based on self-assembled mechanisms, which means that the QDs are randomly distributed on the epitaxial wafers and pose a challenge to the deterministic fabrication process for integrating them with waveguides. For the second, the coherence of photons emitting from any two QDs is generally too low to satisfy the requirement for scalability. A promising solution to break these bottlenecks will rely on the development of site-controlled QDs (growth and deterministic fabrication) along with coherence control, which will be the primary focus of this review.

1.3. Characteristics of S-QD SPEs

Several key characteristics are used to evaluate the performance of single-photon emitters (SPEs), including brightness, quantum efficiency, purity, and indistinguishability (coherence). Each parameter corresponds to a specific measurement technique. However, some papers appear to confuse the purity and indistinguishability [58], possibly due to similarities in their measurement processes. Therefore, it is important to clarify these parameters and their corresponding measurement methods.

Brightness is defined as the emission rate, typically measured in photon counts per second (cps) coupled into the desired optical mode. An SPE with high brightness is crucial for practical applications, such as quantum computation and communication, for faster data transmission and more efficient quantum operation [59]. High brightness also enhances the efficiency of quantum metrology and sensing by providing stronger and more reliable photon signals [60]. Brightness is closely related to (but not equal to) quantum efficiency. A high quantum efficiency is critical for deterministic single photon emission, where one photon is expected under each excitation. The setup for measuring brightness/quantum efficiency is shown in figure 3(a), where a single photon detector (SPD) is utilised together with an electronic readout. Under steady-state excitation, photon count rate (emission rate) as a function of time can be recorded (example shown inset of figure 3(a), middle panel) [61], where the potential rate fluctuation resulting from photon blinking could be observed if the SPE is not stable. Under pulsed-laser excitation, a time decay profile can be

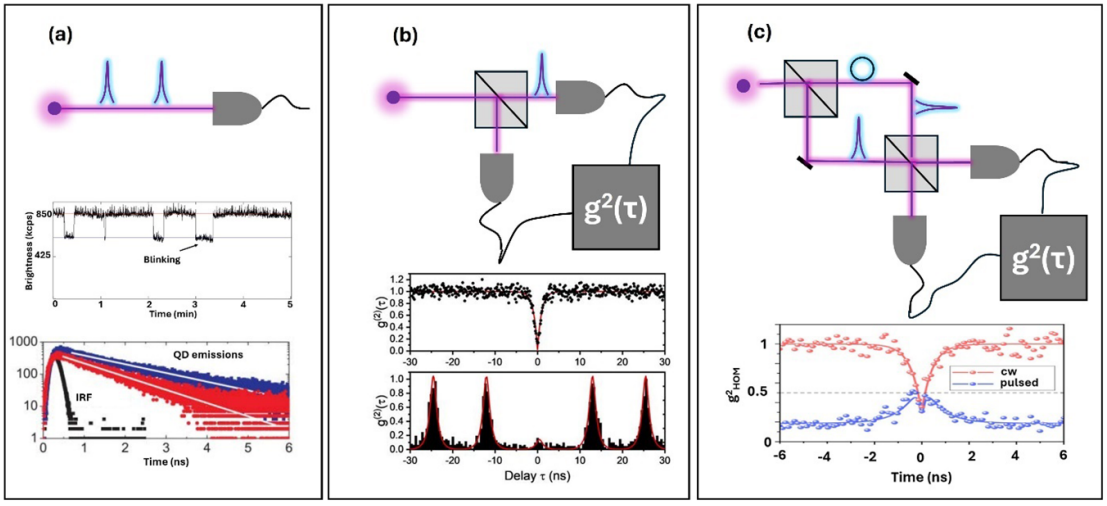

Figure 3. Key characteristics of SPE and related measurements. (a) Schematic of the setup to measure brightness and quantum efficiency (top); measured photon emission rate from a GaN QD with blinking (middle), Reproduced from [61]. CC BY 4.0; TRPL of InAs QD measured with TCSPC (bottom), Reproduced from [62]. CC BY 4.0. (b) Schematic of HBT setup to measure the second-order correlations of a single photon (top); measured $g^2(0)$ of q single photon emission from QDs under cw and pulsed excitations (bottom), Reprinted from [64], with the permission of AIP Publishing. (c) Schematic of HOM setup to measure two-photon interference (top); and measured photon indistinguishability of InAs QDs (bottom), Reprinted with permission from [57]. Copyright (2023) American Chemical Society.

established if the control is equipped with a time-correlated single photon counting (TCSPC) function, as shown in the inset of figure 3(a) (bottom panel) [62]. Such a decay profile (time-resolved photoluminescence, TRPL) will be useful to extract the carrier lifetimes of radiative recombination (τ_r) and non-radiative recombination (τ_{nr}), further for calculating the quantum efficiency by $QE = \frac{\frac{1}{\tau_r}}{\left(\frac{1}{\tau_r}+\frac{1}{\tau_{nr}}\right)}$ [63].

The purity of the SPEs is the probability of one photon emission at a defined time interval. The determination of single photon emission is typically characterised by second-order correlation,

$$g^2(\tau) = \frac{\langle i(t)\, i(t+\tau)\rangle}{\langle i(t)\rangle \langle i(t+\tau)\rangle}$$

where i is the light intensity at the time t and $t+\tau$. It is realised with a Hanbury–Brown and Twiss (HBT) setup [65], as depicted in figure 3(b). The setup contains two SPDs placed after a 50:50 beam splitter, with an electronic coherence control system as the readout. A light beam/pulse containing single photons is sent to the beam splitter. At each detecting event, only one detector will detect the single photon, thus theoretically generating $g^2(0) = 0$. Consequently, the measured correlation curve will present an 'anti bunch' feature, with an example under continuous or pulsed excitation shown in the insets of figure 3(b) [64]. In a practical situation, due to the photon impurity (such as background and imperfect single photon isolation, and sometimes the detector jittering), the $g^2(0)$ will slightly shift away from zero. In other words, a high-purity SPE can be expected when $g^2(0)$ is close to zero.

Coherence is critically required for upscaling SPEs into a quantum system. The coherence is characterised by indistinguishability which is measured with a Hong–Ou–Mandel (HOM) setup [66]. As shown in figure 3(c), the setup comprises a Mach–Zehnder interferometer (MZI) with two 50:50 beam splitters and two SPDs behind the second beam splitter. By tuning the optical delay on one of the beam paths, there is a chance two single photons will be sent to the second beam splitter at the same time. If the two photons are coherent, the interference at the second beam splitter will lead to a quantum statistical probability at the two outputs before each SPD depicted by,

$$|i_1\, i_2\rangle = \frac{1}{\sqrt{2}}\left(|i_{1,2}, 0\rangle_{D1} + |0, i_{1,2}\rangle_{D2}\right)$$

where i_1, i_2 are the light sent to the beam splitter, $D1$, $D2$ are the two channels in front of each detector. After the interference, the two coherent photons will enter the same channel with equal probability, but they cannot go to different channels separately. This indicates that only one detector will receive the incident photon energy, generating a $g^2(0) = 0$ and an 'anti-bunch' curve like the HBT measurements (an example

shown inset of figure 3(c)) [57]. If the two photons are not perfectly coherent, the $g^2(0)$ value will slightly deviate from zero. It is worth noting that purity and indistinguishability measurements have very similar curves, but their measurement methods and physics are different.

2. Fabrication of site-controlled S-QDs

Various fabrication approaches have been developed to achieve the site-controlled S-QDs. Generally speaking, they can be categorised into two groups: epitaxial growth and post-growth fabrication. For epitaxial growth, the pre-patterned substrate could be used for selective area growth; or applying a periodic external driving force (e.g. laser or ion beams) to interfere with the *in-situ* growth dynamics [67–108]. Besides, deterministic fabrication of S-QDs can also be realised by etching down epitaxial layers, with each patterned area containing a single QD [109–138]. Accordingly, this paper will review the fabrication of S-QDs based on the following three primary approaches,

2.1. Epitaxial growth on patterned substrates

The most straightforward method to achieve site-controlled S-QDs could be the growth of semiconductor materials on a patterned substrate. From the growth dynamics point of view, the nucleation process is described at the designated area of the substrate, induced by the *ex-situ* fabricated patterns.

One commonly used method is the direct growth on a pre-patterned dielectric material coated on a substrate. The general process involves depositing dielectric materials (e.g. SiO_2 and SiN) on the substrate, followed by opening the growth window by lithography methods with a critical feature on ∼10 nm. Elarde *et al* deposited 10 nm SiO_2 film on GaAs substrate, which was patterned by electron beam lithography (EBL) [68]. Wet etching was subsequently employed to selectively etch away the mask layer and expose the substrate for the growth. Compared with ion bombardment by dry etching, wet etching will not destroy the crystal lattice on the surface of the substrate. Then the site-controlled InGaAs QDs were successfully selectively grown from the lateral triangular-distributed holes with a diameter of 45 nm by MOCVD. The authors have fabricated their site-controlled QDs into a lateral diode, from which a clear collective dot emission at 1080 nm with a line width of 55 meV has been observed at room temperature. Apart from the conventional EBL, other techniques have also been developed at similar resolutions but at a lower cost. Tommila *et al* reported a template fabricated by nanoimprint lithography (NIL) with hole diameters from 90 to 150 nm (figure 4(a)) [70]. Squarely arrayed InAs QDs were realised by MBE growth. From the AFM measurement (figure 4(a)), 19 individual QDs are grown from 25 holes (76%); whilst some of the holes contain 0, 2 or 3 dots. The room temperature PL measurements indicated the ground state and first excited state recombination peaks corresponding to 1091 and 1039 nm. From the low temperature (20 K) μ-PL measurements, the line width from sing QDs was determined to be 100 μeV. Li *et al* fabricated a patterned SiN mask on GaAs substrate patterned by block copolymer lithography [76]. In this method, the authors first deposited a 15 nm SiN on the substrates. Then the monolayer copolymer nanospheres were fabricated on the surface by spin coating, with a hexagonally ordered distribution. The pattern was then transformed into the growth substrate by dry etching the copolymer. As shown in figure 4(b) (top), the nanoholes with 20 nm diameter and 40 nm centre-to-centre space form a 2D hexagonal lattice. The site-controlled GaAs QDs were selectively grown in the nanoholes by MOCVD as shown in figure 4(b) (bottom).

It is worth noting that the mask is not essentially required for the growth after the pattern is transferred to the substrate. In other words, the mask material (resist, metal or dielectric) could be removed before growth. This is because the selective area growth could still happen due to the local strain or local surface energies. For example, Atkinson *et al* have fabricated nanoholes on the GaAs substrate with *ex-situ* lithography and dry etching methods for MBE growth. They observed that over 50% of single-dot occupancy of an array of holes. Nakamura and co-authors reported the MBE growth of QDs on GaAs substrate patterned with nanoholes, with a diameter of 80 nm, depth 25 nm and a pitch of 200 nm (figure 4(c), top) [67]. By repeating the growth of InAs QD layers several times, the vertically aligned InAs QDs can be obtained from the predesigned nanoholes (figure 4(c), bottom), with improved morphology and optical properties. Later, Schneider and colleagues adopted this method to grow accurately spatial distributed QDs with markers, scalable to integrate with devices [83]. For example, the research team has successfully grown single site-controlled QDs on DBRs schematically shown in figure 4(d) [80]. The dots exhibited an emission line width of 100 μeV, $g^2(0) = 0.12$, and QE of 47% [69]. Hartman *et al* fabricated laterally aligned inverted pyramids on GaAs substrate for MBE growth [77, 140, 141]. Due to the self-limiting growth mechanism, In(Ga)As QDs can be grown on the apex of the inverted pyramid, associated with naturally formed quantum wires (QWRs) on top of the QD and quantum wells (QWs) on the sidewall of the pyramid. Such QDs demonstrate the feasibility of being integrated with photonic structures. For example, Dalacu *et al* fabricated a PC cavity coupled to a single dot inside an inverted pyramid, exhibiting a large coherence tunability of >15 meV [142].

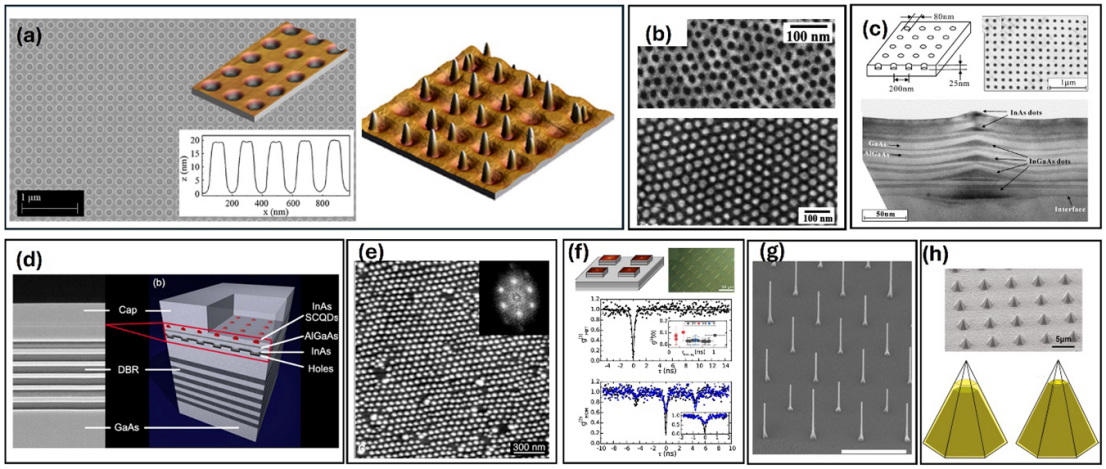

Figure 4. Site-controlled QDs synthesised by epitaxial growth on various pre-patterned substrates. (a) SEM image of periodic nanohole structure fabrication on GaAs substrate (left), AFM of site-controlled InAs QDs grown inside nanoholes on the mask (right); Reprinted from [70], Copyright (2011), with permission from Elsevier. (b) SiN nanohole mask fabricated by copolymer nanosphere lithography (top) and GaAs QDs grown by MOCVD (bottom); Reprinted from [76], with the permission of AIP Publishing. (c) Growth of vertically aligned InAs QDs on a pre-patterned GaAs(001) template, where the mask material was removed before growth, Reprinted from [67], Copyright (2002), with permission from Elsevier. (d) Site-controlled InAs QDs grown on DBR cavities, Reprinted from [80], with the permission of AIP Publishing. (e) Trigonally distributed PbSe QDs epitaxially grown on a mask-free PbEuTe substrate by engineering the local strain, From [139]. © The Authors, some rights reserved; exclusive licensee AAAS. Distributed under a CC BY-NC 4.0 license http://creativecommons.org/licenses/by-nc/4.0/. Reprinted with permission from AAAS". (f) Strain-induced growth of InGaAs QDs on site-controlled mesas (top), with a high purity of $g^2\,(0) = 0.026 \pm 0.026$ and indistinguishability of $(87.1 \pm 9.7)\,\%$ (bottom); Reproduced from [90]. CC BY 4.0. (g) SEM image of the InAsP QD embedded in an InP nanowire grown by selective-area VLS epitaxy; Reprinted with permission from [88]. Copyright (2012) American Chemical Society. (h) SEM image and schematic of selective area grown InGaN QDs in GaN hexagonal pyramids; Reprinted with permission from [93]. Copyright (2011) American Chemical Society.

The local strain on the surface of the substrate could critically impact the nucleation. Therefore, periodic stressing domains on the substrate will be useful for the site-controlled QD growth. In an early work, PbSe(dot)/PbEuTe strain layers were epitaxially grown by MBE, where the stacking of the dots automatically forms a face-centred cubic (fcc) lattice [139, 143, 144]. The vertical elastic interaction of the strain 3D structure will form new nucleation centres for the topmost QDs, which show a laterally trigonal distribution as shown in the SEM in figure 4(e). Strittmatter and colleagues created laterally aligned $Al_xGa_{1-x}/As/AlO_x$ stressors on GaAs substrate by partial oxidation of AlGaAs (the same approach for fabricating the apertures in VECELs) [101, 145, 146]. Subsequently, site-controlled InAs QDs can be grown on top of such stressors. With this method, Groβe *et al* obtained high-quality site-controlled InGaAs QDs on top of DBRs (figure 4(f), top) with extremely narrow linewidth 54 μeV for exciton emission, 35 μeV for biexciton emission and (resolution limited) 27 μeV for charged exciton emission [90]. The emitting photons exhibit a high purity of $g^2\,(0) = 0.026 \pm 0.026$ and indistinguishability of $(87.1 \pm 9.7)\,\%$ (figure 4(f), bottom).

Dot-in-wire is a special group of SPEs, with the advantages of natural isolation of QDs from the nearby environment, high photon extraction efficiency and a defined emission direction. Two ways are often utilised to grow site-controlled dot-in-wire structures, selective area growth with a dielectric mask or vapour–liquid–solid (VLS) growth with a metal mask. For example, Heinrich *et al* fabricated periodic Au patterns on GaAs substrate using EBL lithography. The GaAs dot-in-wire structure array was successfully achieved with MBE, with a narrow line width down to 95 μeV and single photon correlation of $g^2\,(0) = 0.46$. [84] Later, the authors observed a high brightness of 460 kps, a purity of $g^2\,(0) = 0.01$ and a long coherence time of up to 1.2 ns in this unique structure [106]. Dalacu *et al* reported an ultra-purity InAsP dot in InP wire grown with the same mechanism (figure 4(g)), exhibiting a narrow linewidth of 30 μeV and $g^2\,(0) < 0.0\,1$ [88] The group also demonstrated a wavelength tunable single QD emission from 880 to 1550 nm by changing the thickness of a-Si coating layer on the nanowires, whilst maintaining a high brightness of 0.4–35 kps and a high purity of $g^2\,(0) < 0.02$ [92]. In order to control the morphology and reproducibility of the QDs in a nanowire, Tatebayashi *et al* adopted a catalyst-free growth InAs dot in GaAs wire on a GaAs substrate with SiO_2 mask using MOCVD [85]. By controlling the growth parameters, disk-like QDs are formed inside the nanowire, exhibiting a narrow line width of 87 μeV and a $g^2\,(0) = 0.11$. Similar growth methods have been used to grow core-shell dot-in-wire structures with line widths of 162 μeV and purity $g^2\,(0) = 0.18$ [103]. An additional advantage of the dot-in-wire structure is that the

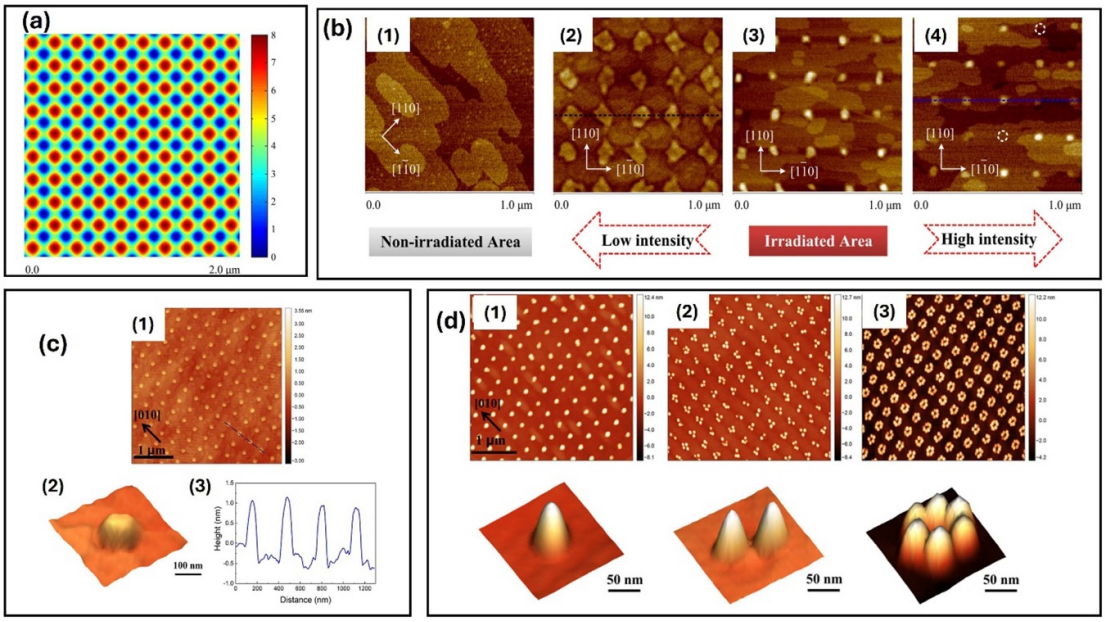

Figure 5. Recent progresses in *in-situ* epitaxial growth of site-controlled QDs with the assistance of laser interferences on planar substrates. (a) Simulated four-beam laser interference patterns for *in-situ* QD growth. (b) AFM images of the surface morphology of site-controlled InAs QDs grown under different irradiation intensities. Reprinted from [150], with the permission of AIP Publishing. (c) AFM images of the 2D (1), 3D (2) morphology and profile (3) of site-controlled InAs QDs by *in-situ* growth under laser interferences. (4) controlling the number of QDs grown on each laser interference spot. Reprinted from [154], with the permission of AIP Publishing.

morphology can be defined by the mask's shape as demonstrated by Foster *et al* [91, 97], leveraging the polarisation control of the emission photons.

Besides the above-mentioned III-As/P materials, similar growth methods were developed for growing III-nitride site-controlled QDs (example shown in figure 4(h)) [81, 82, 89, 93–97, 102, 105, 147, 148]. Pérez-Solórzano *et al* reported the growth of a hexagonal pyramid of GaN grown on a SiO_2 patterned InGaN/GaN substrate [81, 102]. At the apex of the pyramid, InGaN QDs were recognised by the CL and PL measurements. Moreover, bright emission under coherent excitation [148], directional and highly polarised emission [87, 93, 97], high purity single photons [94] and transferable site-controlled QDs [96] have been achieved in III-Nitride dots. Site-controlled dot-in-wire structures were also developed in the III-Nitride material system. For example, Choi *et al* have studied the GaN QDs grown in Al(Ga)N wires grown by MOCVD, with a collective emission line width of 2.7 meV [71, 82], followed by further work showing a high purity of single photon emission of $g^2(0) = 0.32 \pm 0.11$ [105]. In order to improve the morphology and reproducibility of III-nitride QDs, Deng et.al developed GaN/AlN dot-in-wire structure on non-polar AlN/Si substrate by MOCVD [89]. The dot exhibits a disk-like structure, with high single photon purity of $g^2(0) = 0.19$ and a quantum efficiency of 31.1%.

2.2. *In-situ* growth

In-situ growth process does not involve any pre-growth fabrications on the substrate, thus maintaining a high purity of the dots, which facilitates the subsequent device processing. Ohkouchi and colleagues developed an *in-situ* In dot array fabrication using a UHV-AFM system [72]. The GaAs substrate with the In dot arrays was then transferred into the MBE chamber connected to the UHV-AFM system. The indium facilitated VLS growth and InAs dot can be selectively grown [149]. It is a reproducible process, though it may not be favoured by the large-area growth required by upscaling the dots. Recently, Zhang *et al* and Wang *et al* reported the site-controlled InAs QD *in-situ* growth by MBE, achieved by a four-beam interference on GaAs substrate [150, 151]. In Zhang's work [150], 4 beams are split from a 3rd harmony Nd:YAG laser with an emission wavelength of 355 nm, which were arranged in the four viewport of the MBE with an angle of 60°. Figure 5(a) displays the simulated interference pattern, where periodic high-intensity spots were formed. Due to the interaction between laser energy and the InGaAs wetting layer, periodic nanoislands are generated on the 'hot spot' to form seed areas for the subsequent QD growth. Figure 5(b) shows the nanoislands formed at different areas on the substrate, namely no interferences, and with interferences at low to high intensities (from left to right). Clearly, periodic InAs QDs formed on the substrate, and their morphologies are related to the intensity of the laser. Want *et al* have systematically studied the interference

Table 2. A summary of the epitaxial growth methods of site-controlled QDs.

Growth methods	Advantages	Challenges
Growth on substrate with dielectric patterns	• Easy for fabrication and growth • Potential for large-area growth • Various pattern shapes for controlling QD morphology • Dot-in-wire structure	• Influence of fabrication error on QD optical properties • Introduce external material to the growth chamber
Growth on patterned substrate W/O dielectrics	• No additional material was introduced to the growth chamber	• Potential material growth in the non-patterned area
VLS growth with metal patterns	• Fast growth rate in the vertical direction • Dot-in-wire structure	• Potential metal interdiffusion to the grown structure and contamination to the chamber
In-situ patterned growth	• Less contamination	• Low fabrication rate and not suitable for large area growth
In-situ Laser-induced growth	• Zero contamination • Good uniformity	• A new technique requiring further study in growth dynamics and morphology control for QD-SPEs

patterns by changing the parameters of the laser beams and improved the beam using beam shapers [151, 152]. They have achieved high-quality InAs dot arrays, forming lateral square lattice with a pitch of 300 nm on GaAs substrate (figure 5(c)) [153, 154]. By manipulating the growth parameter, single or multiple dots can be grown on the selected area (figure 5(d)) [154].

Table 2 shows a summary of the growth methods of site-controlled QDs associated with their advantages and challenges. Most of the site-controlled QD-based SPEs are fabricated by the growth on patterned substrates, which is straightforward and simple. But the optical properties of QDs need to be further improved to compete with the self-organised grown ones on flat substrates. In comparison, the *in-situ* growth assisted with laser beam interference is promising, but it requires further understanding in growth dynamics to realise high-performance QD-based SPEs.

2.3. Post-growth fabrication

Many deterministic fabrication methods have been developed to locate a single QD on a self-assembly epitaxial wafer. The methods often include registering the position of a single QD followed by top-down device fabrication. One advantage of such methods is that the fabricated device will inherit the good optical properties of the self-assembled QDs (e.g. the line width is often recognised better than the selective-area grown counterparts).

The early works normally utilise microscopy imaging methods (using SEM, AFM etc) to locate a single QD, as a straightforward approach. However, single QDs often buried below the epitaxial layers (e.g. capping layer), which hinders the direct observation by microscopy. To overcome this, Henness *et al* developed a method to grow a tracer QD above the active QD [134]. As shown in figure 6(a) (left), the tracer QD at the top of the epitaxial layer, which can be observed by SEM, has a distinguished different emission wavelength from that of the active QD beneath. With a subsequent locating of the tracer QD by SEM and EBL prepared marker (figure 6(a), right), a single InAs QD was fabricated into a GaAs photonic slab (figure 6(b)), allowing them to observe the large Purcell effect in the weak coupling regime [137] Later, the authors developed an AFM registration method to fabricate a single QD at the centre of a PhC cavity, facilitating the study of photon-cavity mode interactions in the strong coupling regime [136]. Kuruma *et al* has also developed similar approaches enabling the detection of a QD with a sub-10 spatial precision [135].

In order to avoid relying on imaging only the physical presence of a QD and alignment to prefabricated markers, CL-assisted *in-situ* EBL has been developed [122, 126]. Figure 6(c) schematically shows the fabrication process [123]: the CL emission of a PMMA-coated epilayer was first recognised under e-beam illumination. At the target QD position, the e-beam dose will be increased to exposure to the PMMA resist, followed by developing and dry etching to obtain a single QD embedded in a sub-μm mesa. This method allows a direct fabrication of the QDs with a spatial resolution $<$50 nm. Gschrey et.al demonstrated single photon emission of an InGaAs dot-in-mesa fabricated by this method exhibited an ultra-narrow line width of 9 μeV and a purity of $g^2(0) = 0.04$ from the charged exciton emission [123]. Later, Schnauber *et al*

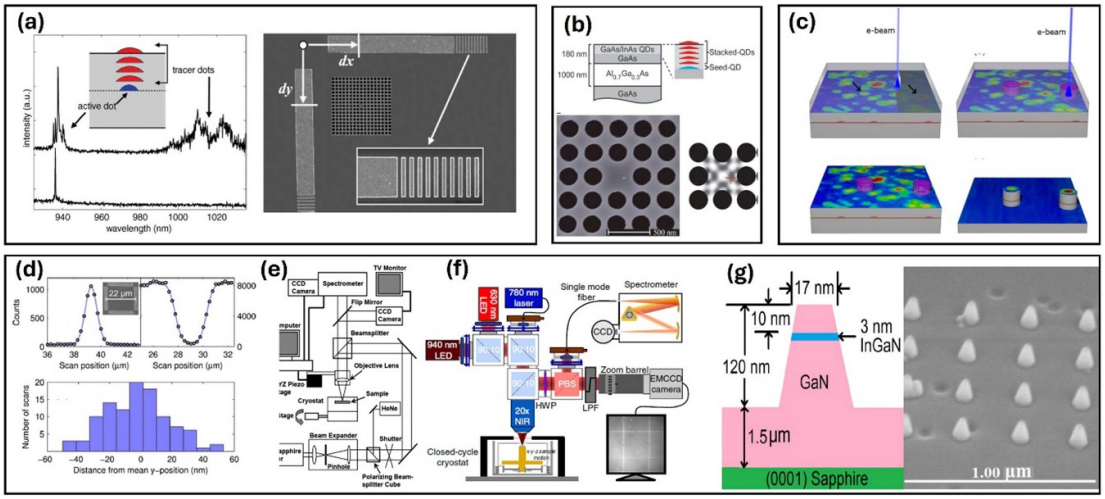

Figure 6. Deterministic fabrication of single QD-based SPEs from self-organised grown epitaxial wafers. (a) The emission spectrum from active and tracer dots under low and high excitation powers (left), and SEM image of a single QD coupled with PhC structure with a position respect to the Au markers (right). Reprinted from [134], Copyright (2004), with permission from Elsevier. (b) Tracer-QD assisted fabrication of an active (seeded) QD into a PhC cavity for strong Purcell enhancement, From [137]. © The Authors, some rights reserved; exclusive licensee AAAS. Distributed under a CC BY-NC 4.0 license http://creativecommons.org/licenses/by-nc/4.0/. Reprinted with permission from AAAS. (c) Deterministic fabrication of a single QD by *in-situ* e-beam lithography equipped with CL, Reprinted from [123], with the permission of AIP Publishing. (d) Positioning single QD with μPL scanning along with a statistical method, achieving a spatial resolution <10 nm, Reprinted from [155], with the permission of AIP Publishing. (e) Schematic of a confocal scanning system for scanning the position of a single QD, Reprinted from [133], with the permission of AIP Publishing. (f) Schematic of a cryogenic photoluminescence imaging system for positioning of QDs with a ∼4.5 nm uncertainty, Reprinted from [121], with the permission of AIP Publishing. (g) InGaN disk-like QD array formed by e-beam lithography patterning and direct dry etching a single QW wafer, Reprinted from [112], with the permission of AIP Publishing.

realised single InAs QD deterministically integrated with SiN waveguides on Si by the same approach [132], and integrated with GaAs waveguide and a multi-mode interference (MMI) coupler [131], demonstrated promising potential of on-chip SPEs for upscaling.

Optical metrology has also been broadly used to determine the position of self-assembled QDs. In this method, the light emission of a target dot will be monitored and aligned to the prefabricated marker. The advantage of this approach is that the emission properties can be selected to couple to the designed photonic structures, thus generating a high device yield. In early works, scanning confocal methods are exploited for deterministic fabrication. Thon *et al* utilised a confocal scan of the QD emission position, which is aligned to the prefabricated Au markers nearby [155]. By using a simulation and average of the emission position with many colonial scan images (figure 6(d)), they achieved a spatial resolution sub-10 nm accuracy to fabricate the target InAs QD into the right position of a PC cavity (for strong coupling) with a success rate of 70%, together with the purity of $g^2(0) = 0.21$ [155]. μPL imaging was also developed to locate a target self-assembled QD. Figure 6(e) shows the schematic setup of μPL imaging system, where the CCD camera was used to determine the position of the QD (by recording its emission) [133]. The authors fabricated the alignment markers around the QD, which facilitated the subsequent PC cavity fabrication to couple the QD. Similarly, an *in-situ* lithography was developed to fabricate InAs self-assembled QDs into a DBR microcavity with a spatial resolution of 50 nm, allowing the observation of cavity QED such as high Purcell factors [129] Similar fabrication can be found in other works, either incorporated into a PC cavity or DBR micro-cavity [120, 124, 125, 155] with a resolution <50 nm. Besides this, Sapienza *et al* have developed a two-colour photoluminescence imaging technique to determine the position of single QDs with respect to the alignment marks (figure 6(f)). Together with the numerical fitting of the position of the emission spot, they have achieved a spatial resolution of <30 nm (<10 nm with immersed lens) [121, 128], allowing the achievement of an SPE with a purity of $g^2(0) < 0.01$.

Direct fabrication, which involves standard lithography and etching but without external positioning methods, was also developed for transforming material (such as QWs) into deterministic dots or dot arrays. For example, Verma and Coleman have reported using HSQ mask (a negative EBL resist) for etching InGaAs single QW epiwafer. A dot array was formed after etching in the $C_6H_8O_7$:H_2O_2 = 50:1 solution with an etching depth of 15 nm [156]. Those QDs with an average diameter of 40 nm show a clearly different

Table 3. A comparison of the deterministic fabrication methods of QDs.

Post-growth fabrication	Advantages	Disadvantages
SEM (or AFM) imaging with alignment markers	• Straightforward fabrication methods	• Less spatial resolution
SEM (or) AFM + tracer QD +markers	• Good fabrication accuracy at 40–50 nm • Fine optical structure fabrication	• Requires a special growth technique
CL-assisted EBL *in-situ* fabrication	• Good spatial resolution (<50 nm) • *In-situ* select optically active QDs • Fine optical structure fabrication	• Unable to judge single photon emission before fabrication
Scanning confocal and μPL assisted fabrication	• High spatial resolution (down to sub-10 nm) • Preselecting QD-SPE with high optical properties • High success rate	• Small scanning area • *In-situ* fabrication limited only to the optical resolution
QD array by lithography and top-down etching	• Easy for fabrication	• Uncontrollable optical properties (surface defects, shape etc.)

emission spectrum compared with the single QW [157]. Later, they measured the single photon emission from an InGaAs QD fabricated with similar methods, with an HBT purity of $g^2(0) = 0.314 \pm 0.03$ [115]. Similar methods involve direct lithography and dry/wet etching also developed by other groups to fabricate deterministic single QDs for III-As and III-P materials [158–160]. Zhang *et al* reported the fabrication of InGaN/GaN QDs by dry etching a single InGaN QW (with In content of 15%) [112]. The process involves employing EBL to define a Cr etching mask, followed by RIE-ICP dry etching. After dry etching and removing Cr, Al_2O_3 was deposited by ALD to passivate the side wall of the QDs [161]. Figure 6(g) shows the morphology of the etched QDs, the cone structure consists of a disk-like InGaN dot with a thickness of 3 nm, exhibiting a line width of 6 μeV and single photon emission of $g^2(0) = 0.18$ at 10 K and $g^2(0) = 0.38$ at 90 K. The research team further improved the morphology of the QD structure and has realised polarisation control, electrical injection and brightness enhancement with plasmonic structures [110, 111, 114, 116].

There are also other post-growth fabrication methods for fabricating QDs and locating a single QD. Such as the early work using Ion beam sputtering a GaSb film grown AlSb to form GaSb dot arrays [117], and fabricating a small aperture to allow single QD emission [113]. Such methods fall outside the scope of this review, due to the limitations in the yield and scalability.

Table 3 shows a comparison of the post-growth deterministic fabrication methods for QD-based SPEs. In summary, the SEM or AFM imaging with external markers normally has a limited resolution for achieving perfect QD-photonic structure coupling. With an additional tracer QD or CL, a spatial resolution with 50 nm can be achieved for positioning a single QD. In comparison, optical methods using μPL or confocal allows the selection of the QDs with desired optical properties, and a high spatial resolution down to sub 10 nm, which enables the precise QD-photonic structure coupling toward high-performance SPEs.

3. Optical properties of site-controlled QDs

3.1. Photon emission from single-QD system

As a bare QD emits photons to free space without a preferred optical mode, it is unlikely directly applicable to quantum information science and technology. Therefore, single QDs are often engineered into a photonic structure to deliver the single photons into designated optical modes. Commonly used photonic structures include PC waveguides and cavities, microcavities (e.g. DBR and microdisk), and waveguiding devices (e.g. ring resonators, waveguides).

PhC are fabricated by periodically adjusting the optical index in a planar material (often by fabricating air hole arrays), so that photonic band structure can be achieved between energy (frequency) and momentum (in analogy to the electronic band structure in solids). As a result, light with a certain frequency (wavelength) is inhibited from propagating in the PhC. One of the advantages of PhC is the strong optical confinement, which enables the observation of strong light-matter interactions. Therefore, it is a good host for single QDs. PhC waveguide indicates a PhC with missing one line of air holes (figure 7(a)) [162], where light can only propagate along this line. Many groups have fabricated QDs into PhC waveguides to study

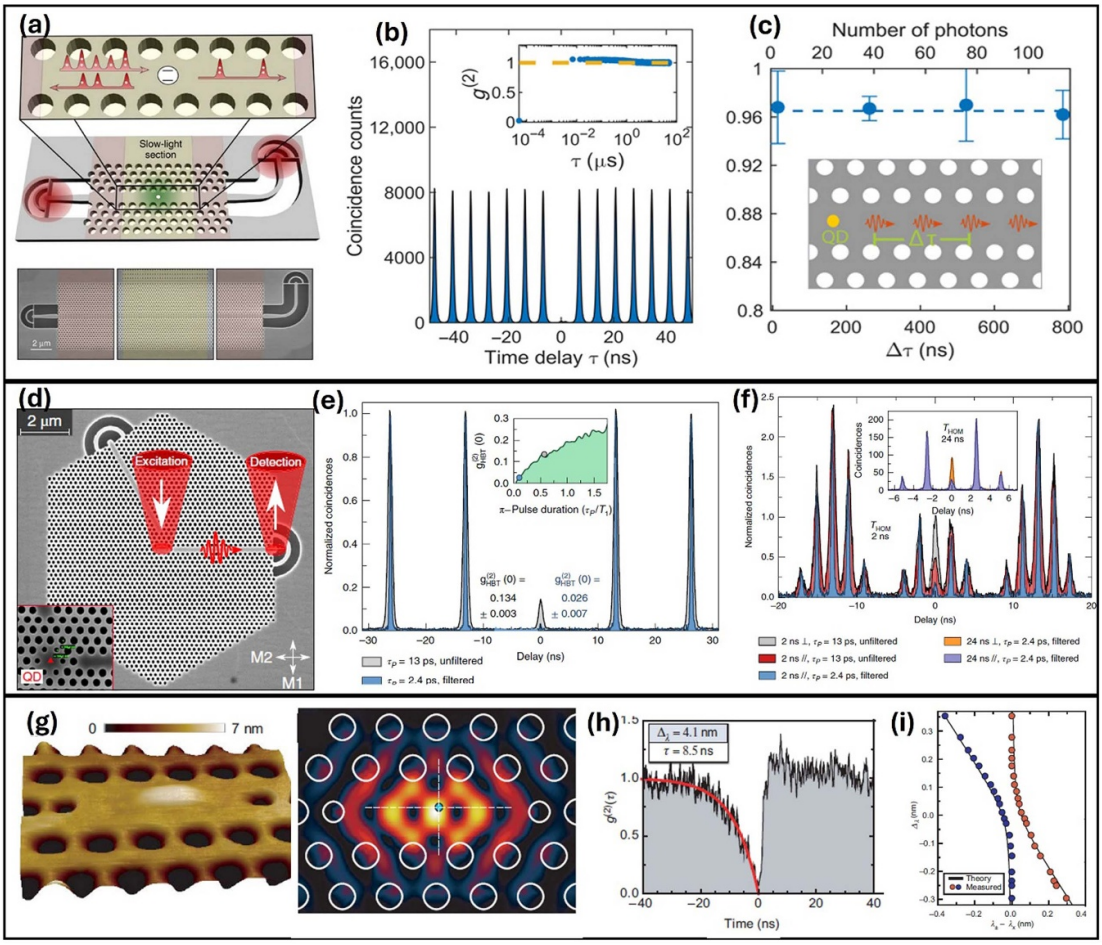

Figure 7. Single QD coupled with PhC structures. (a) Schematic and SEM image of a single quantum dot coupled with a PhC waveguide. Reproduced from [162]. CC BY 4.0. (b) High purity of $g^2(0) = 0.015 \pm 0.005$ achieved in a QD-PhC waveguide system. (c) Photon indistinguishability between photon pairs reaching >96% by measuring 115 photons in a QD-PhC system. From [166]. © The Authors, some rights reserved; exclusive licensee AAAS. Distributed under a CC BY-NC 4.0 license http://creativecommons.org/licenses/by-nc/4.0/. Reprinted with permission from AAAS. (d) SEM image of an InAs QD integrated H1 PhC cavity. (e) HBT measurement of single-photon purity with π-pulse excitation under using 13 ps (grey) or 2.4 ps (blue) pulses. Inset shows the $g^2(0)$ value as a function of pulse duration. (f) HOM visibility under different pulse excitation, with a best value of 93.9 ± 3.3%. Reproduced from [167], with permission from Springer Nature. (g) AFM topography of a L3 PhC nanocavity coupled with a single InAs QD (left), and optical mode inside the cavity (right). (h) Cavity–exciton anticorrelation measurement shows an asymmetric near-zero value at single photon level. (i) The anti-cross nature of the cavity mode and the excitons by detuning the cavity mode indicates reaching a strong coupling regime. Reproduced from [136], with permission from Springer Nature.

quantum photonics such as chiral emission, slow light, spin-orbit coupling and so on [162–165]. A recent report has demonstrated an InAs QD deterministically fabricated into GaAS PhC waveguide achieved an ultrabright single photon emission of 122 million per second, corresponding to an on-chip source efficiency of 84% [166]. The purity achieved $g^2(0) = 0.015 \pm 0.005$ with almost no observable blinking (figure 7(b) and inset). By checking 115 photons, the indistinguishability realised a value of 96% (figure 7(c)) [166]. PC cavities are also popular for hosting single QDs. Two types of PC cavities are often studied: H1 cavity with one missing hole (figure 7(d)) and L3 cavity with three missing holes in a line (figure 7(g)). Liu *et al* reported an H1 PhC cavity coupled with a PhC waveguide (figure 7(d)) [167]. Owing to the strong optical confinement, a strong Purcell factor (enhancement of the brightness) of 43± 2 has been observed. Under π -pulse excitation with a grating filter (to remove the system birefringence), a photon purity of $g^2(0) = 0.026 \pm 0.007$ and an indistinguishability of 99% were observed (figures 7(e) and (f)). Hennessy *et al* deterministically integrated an InAs QD within an L3 PhC cavity (figure 7(g)), where they observed a strong cavity mode related single photon emission with $g^2(0) \sim 0$ (figure 7(h)) [136]. Moreover, a clear anti-crossing was obtained, indicating a strong coupling regime was achieved (figure 7(i)) [136]. Such a QD-cavity coupling system is a good candidate for studying cavity QED, for developing quantum devices such as quantum memory, gates and switches [42, 168–170].

PhC cavity requires delicate device fabrication including the control of the air hole size (often at ∼100 nm) and period as well as the precise placement of the QDs, which has a stringent tolerance to the

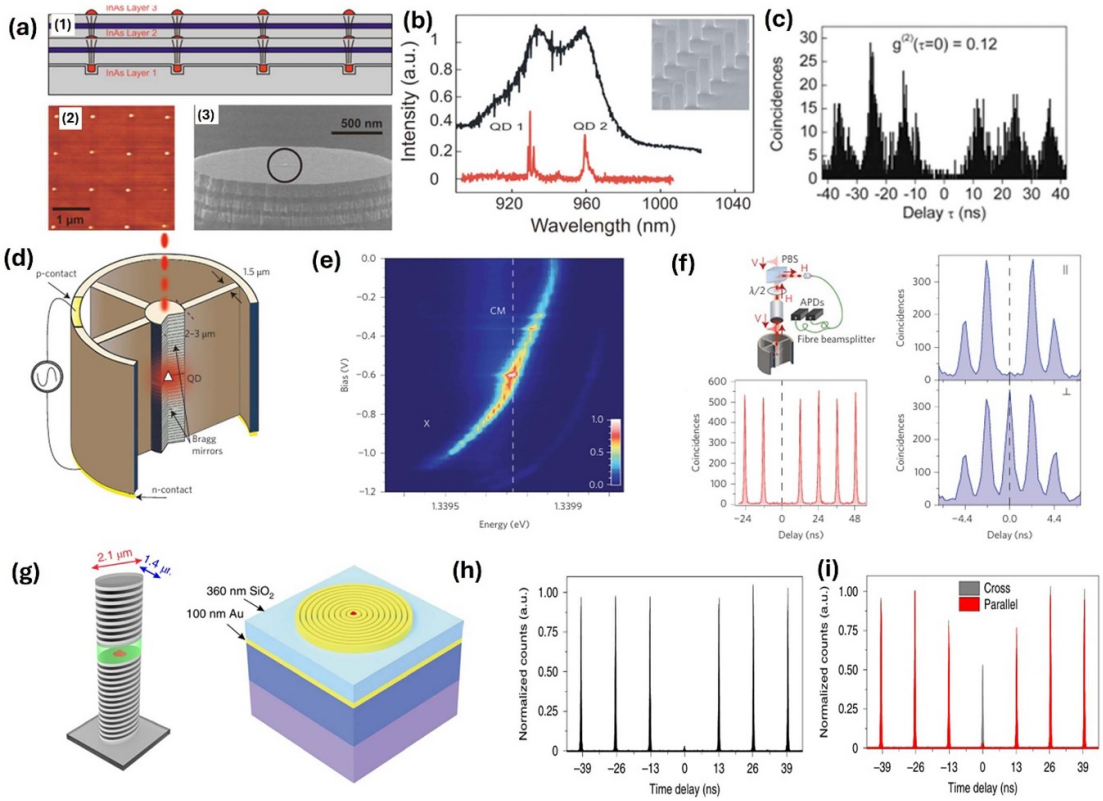

Figure 8. Single QDs coupled with micro-cavities and optical meta-surfaces. (a) Schematic and morphologies (AFM & SEM) of site-controlled InAs QDs grown on GaAs/AlAs DBR microcavity. (b) The emission of the ensembled QDs without DBR cavity (black) and emission from QD coupled with a DBR cavity (red). (c) HBT measurement of the charged exciton emission on-resonance with the cavity mode with $g^2(0) = 0.12$. Reprinted from [79], with the permission of AIP Publishing. (d) Schematic of an InGaAs QD coupled with a DBR designed in a p–i–n structure. Emission wavelength can be tuned by the external bias through Stark effect. (e) Emission intensity as a function of bias and energy, showing a tuning range of ∼4 meV of the exciton emission. (f) HBT measurement of a QD-coupled the p–i–n DBR cavity at 0.75π pulse excitation showing $g^2(0) = 0.0028 \pm 0.0012$; and the HOM measurement parallel/cross polarised photon indistinguishability (right). Reproduced from [174], with permission from Springer Nature. (g) Schematics of an InGaAs QD coupled to an elliptical DBR cavity (left) and an elliptical planar resonant DBR grating structure (right), to extract one of the preferred polarisations. (h) HBT measurement of QD-elliptical DBR cavity showing $g^2(0) = 0.025(5)$. (i) HOM measurement of QD-elliptical DBR cavity showing photon indistinguishability of 0.975(6). Reproduced from [51], with permission from Springer Nature.

fabrication imperfections. In contrast, DBR microcavity (e.g. micropillars) is a vertical structure, where the QD can be placed at the centre (electric field anode) between the top and bottom DBRs by epitaxial growth. While the cavity mode can be tuned by varying the horizontal dimensions. Therefore, the fabrication of DBR cavity-coupled QDs is relatively easier. Schneider *et al* reported the site-controlled growth InAs QDs on seeded QDs on a patterned AlAs/GaAs DBR mirror, where the topmost QDs are distinguishable (figure 8(a)) [79]. The QDs are further grown in the centre of a full DBR cavity, with top and bottom 12 and 25 pairs, and a lateral size of 2 μm in diameter. Clear emissions from the top and bottom QDs with a different wavelength and narrow linewidth were observed, in comparison to the QDs without being fabricated into DBR microcavities (figure 8(b)). Moreover, a single photon purity of $g^2\,(0) = 0.12$ has been realised (figure 8(c)) [79]. Gazzano and colleagues reported deterministically fabricated InGaAs QD in an AlAs/GaAs DBR cavity with brightness up to 0.79 ± 0.08 per excitation pulse, purity of $g^2\,(0) \leqslant 0.15$ and invisibility of $82 \pm 10\%$ [25]. The performance of such quantum emitters was further improved including enhanced extraction efficiency (up to 85%) and electrically detuning coherence (range = 1.4 meV) [171–173]. Figure 8(d) displays a micropillar with QDs fabricated into a DBR cavity in a p–i–n structure, facilitated with an external bias to turn the coherence (∼4 meV range, figure 8(e)) [174]. Under resonant excitation, the photo purity achieved a $g^2\,(0) = 0.0028 \pm 0.0012$ and indistinguishability (same polarisation) of $99.56 \pm 0.45\%$ (figure 8(f), left), with a photon extraction of 65%. For cross-polarisation photons, the measurement shows a clear vanishing interference (figure 8(f), right) [174]. In order to solve the problem of 50% efficiency loss due to cross-polarisation, Wang *et al* proposed an elliptical DBR pillar (and an elliptical Brag grating structure) to break the symmetry for extracting one preferred polarised emission to another (figure 8(g)) [51]. In such devices, they have demonstrated a polarised single photon QE of $60 \pm 2\%$ and $58 \pm 2\%$ for the

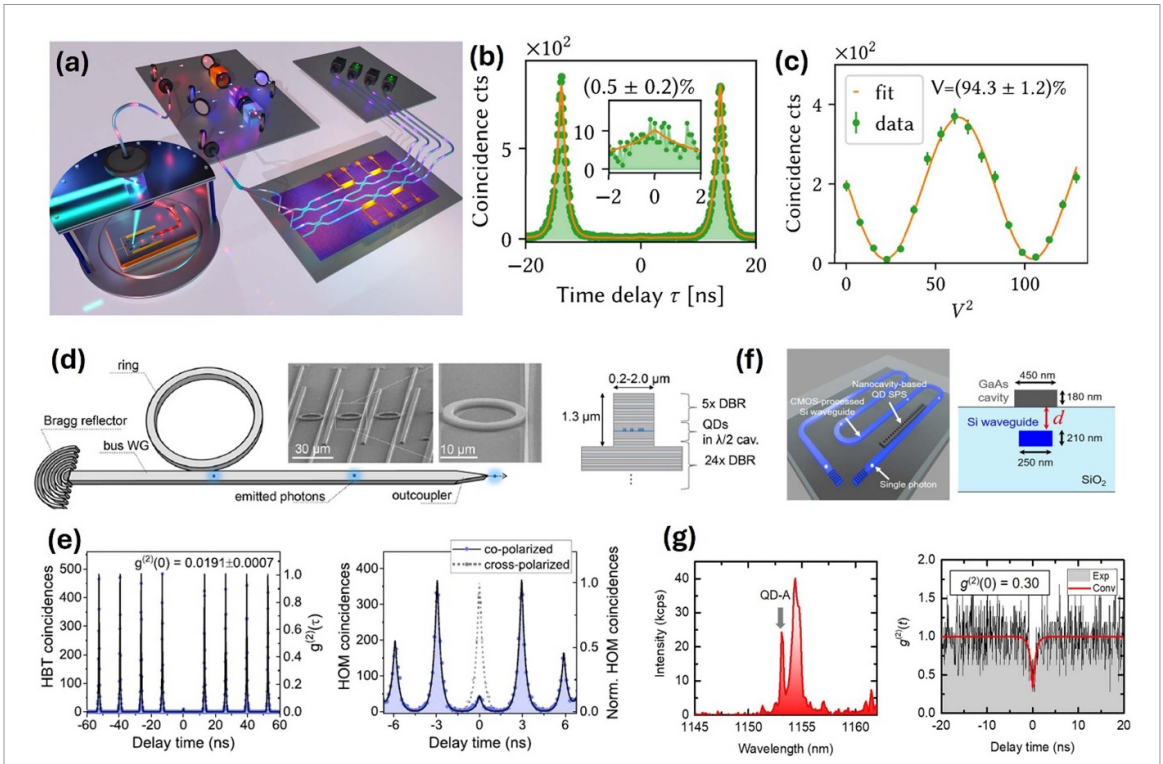

Figure 9. QD integrated with Si photonics. (a) Schematic of a QD SPE coupled to a SiN photonic chip through an external fibre and free space demultiplexing system. (b) HBT measurement on the SiN chip, with a purity of $g^2(0) = 0.005$. (c) HOM measured using an on-chip MZI circuit with a photon visibility of 94.3 ± 1.2%. Reproduced from [179]. CC BY 4.0. (d) Scheme and SEM image of DBR coupled with a single QD integrated with a waveguiding ring resonator; emitted photons are collected from the side facet of the structure within the tapered out-coupler (left); DBR waveguide cross-section with marked layers (right). (e) HBT measured photon purity of $g^2(0) = 0.0191 \pm 0.0007$ (left); and HOM photon indistinguishability of 0.95 ± 0.02 (right). Reprinted with permission from [180]. Copyright (2020) American Chemical Society. (f) Schematic of a nanocavity-based QD SPE transfer-printed on a CMOS-processed silicon waveguide with glass cladding (left); illustration of the device cross section (right). (g) PL spectrum at output port (left); HBT measurement with $g^2(0) = 0.30$ at the output port (right). Reprinted from [182], with the permission of AIP Publishing.

elliptical DBR and Brag grating devices, respectively. The single photon purity of the two devices is 0.975 ± 0.005 (0.991 ± 0.003) and indistinguishability is 0.975 ± 0.006 (0.951 ± 0.005) for the DBR (elliptical Brag grating structure), as shown in figures 8(h) and (i) [51].

Other types of cavities could also be used for hosting single QDs, such as FP cavity, microdisk, and metallic plasmonic cavity [175–177]. As the working principle is similar to the above examples, this paper will not elaborate on the details. However, the single QDs integrated with dielectric waveguides (not the PhC waveguides as mentioned above) are particularly interesting, because they hold the promise to develop on-chip SPEs, in line with the fast-developing Si photonics. Schnauber *et al* has demonstrated an *in-situ* EBL method to fabricate single III–V QDs integrated with waveguides, and the heterogeneous integration of InAS/GaAs QD nanobeam cavity with SiN waveguides on Si [131, 132]. The III–V nanobeam cavity equipped with an optical taper to transit the optical mode into SiN waveguide, they have demonstrated a purity of 0.11 [132]. The authors have also demonstrated the coupling of sing III–V QD with SiN PICs containing photonic ring resonators and beam splitters, where they obtained an ultra-high-purity of $g^2(0) = 0 \pm 0.13$ and a coupling efficiency $\eta = 23 \pm 3\%$ [178]. Want *et al* reported interfacing III–V QD in PhC cavity and programmable SiN PIC platform coupled by optical fibres with a measured coupling efficiency of 21.5% (figure 9(a)), where they observed photon emission from the SiN PIC with a high purity of $g^2(0) = 0.5 \pm 0.2\%$ and a high coherence 94.3 ± 1.2% (figures 9(b) and (c)) [179]. Dusanowski and co-authors have developed an InAs/GaAs QD monolithically integrated into a ring resonator, which was coupled to a bus waveguide with one end of a full DBR reflector and another side of an out coupler, as shown in figure 9(d) [180]. The device allowed them to observe a 4-fold (Purcell factor) enhanced brightness, with a photon purity of $g^2(0) = 0.0191 \pm 0.0007$ and indistinguishability of 95 ± 2% (figure 9(e)) [180]. The hybrid integration based on the 'pick-and-place' method has also been developed recently for coupling QDs into dielectric waveguides. Zadeh *et al* demonstrated an integrated SiN waveguide with InGaAs QD-in-InP wire, where the nanowire (with a sharp tip) guides the single photon emission into the SiN waveguide [181]. The

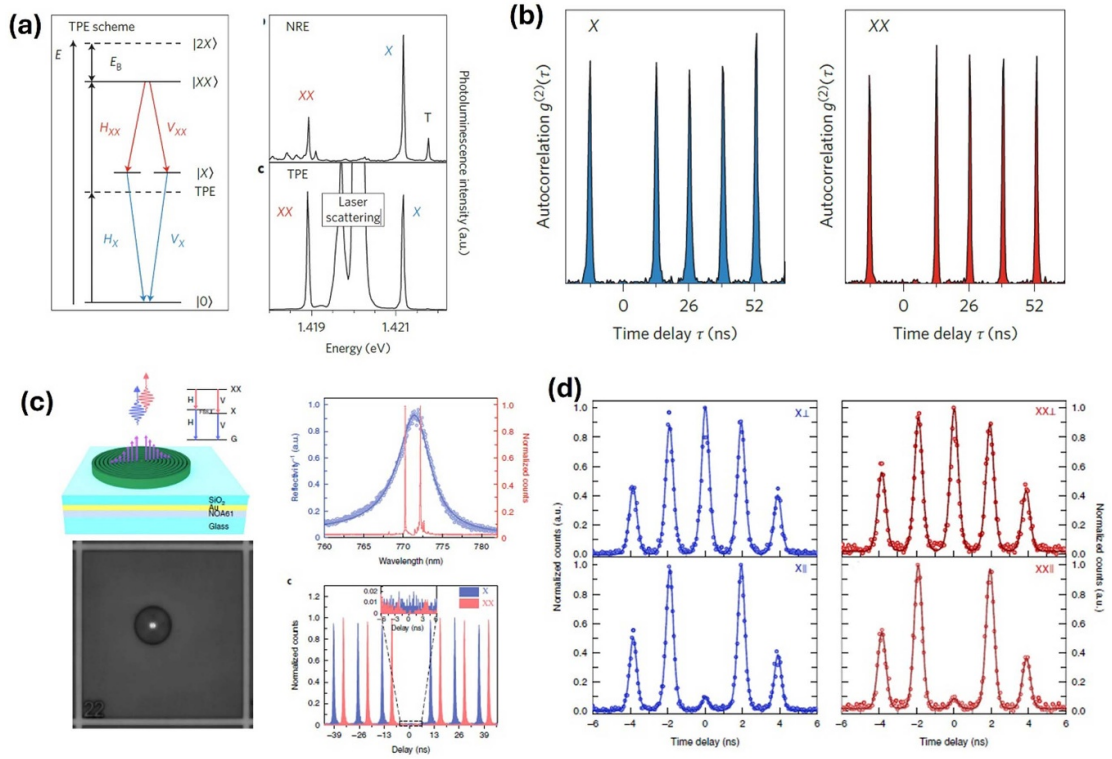

Figure 10. Entangled photon pair generation from compound QDs photonic structures. (a) illustration of TPE for photon pair generation process (left); above-bandgap excitation spectrum and emission spectrum of InGaAs QD under biexciton direct TPE (right). (b) HBT purity of the exciton $g_X^2(0) = 0.004 \pm 0.018$ (left) and biexciton $g_X^2(0) = 0.003 \pm 0.018$ (right) by considering the detector's dark count contribution. Reproduced from [186], with permission from Springer Nature. (c) schematic and fluorescence image of a GaAs QD coupled to a circular Bragg resonator on highly efficient broadband reflectors (CBR-HBR, left); QD emission spectrum in the CBR-HBR cavity and HBT purity of $g^2(0) = 0.001 \pm 0.001$ and $g^2(0) = 0.007 \pm 0.001$ for exciton and biexciton emission (right). (d) HOM visibility achieving 0.901(3) and 0.903(3) for exciton (blue) and biexciton (red) emissions. Reproduced from [187], with permission from Springer Nature.

authors have observed a coupling efficiency 24.3 ± 1.7%, and a high photon purity of $g^2(0) = 0.07 \pm 0.07$ with a line width of 3.45 ± 0.48 GHz [181]. Katsumi *et al* reported the integration of an InAs QD in GaAs nanobeam cavity with Si waveguide on SOI by micro-transfer printing method (figure 9(f)) [182]. The measured coupling efficiency is as high as 70% when the distance between GaAs cavity and the Si core is 450 nm (figure 9(f)), and purity of $g^2(0) = 0.03$ when coupled into the waveguide (figure 9(g)) [182]. In another work, the research team has achieved the strong coupling regime with QDs on a Si photonic chip by the same fabrication methods [183].

Entangle photon emissions were also observed in site-controlled QDs based on the cascaded emission of bi-excitons or higher. Such photons exhibit polarisation entanglement. Due to the existing fine structures and binding energy the emission of exciton and bi-exciton photons often show a slightly different energy, which can be tuned by growth, external magnetic field or electric field [45, 184]. Braun *et al* has observed strong polarised cascaded two-photon emission from site-controlled InP/GaInP dots along [0–11] direction [185]. The bi-exciton binding energy and total fin structure splitting are 4.15 meV and 237 ± 5 μeV. They also observed the purity for exciton $g^2(0) = 0.08$ and bi-exiton $g^2(0) = 0.48$, a cross-correlation between them with a minimum of 0.61 and a maximum of 1.41 [185]. In order to enhance the performance, Müller *et al* reported the generation of on-demand indistinguishable polarisation-entangled photon pairs through two-photon resonant excitation (figure 10(a)) [186]. The corrected purity of exciton and bi-exciton emissions are $g^2(0) = 0.004 \pm 0.018$ and 0.003 ± 0.018, with the indistinguishability is 84 ± 5% and 69 ± 4%, respectively (figure 10(b)) [186]. Liu *et al* has fabricated concentric Brag gratings surrounding a GaAs QD (figure 10(c)), where they have realised high purity of $g^2(0) = 0.001 \pm 0.001$ and 0.007 ± 0.01 for exciton and bi-exciton emissions, with indistinguishability of 0.901(3) and 0.903(3), respectively (figure 10(d)) [187]. The device exhibits a pair efficiency of 0.65(4) and a high entanglement fidelity of 0.88 (2). Wang *et al* used a slightly elliptical Brag grating realised pair efficiency of 0.62, photon indistinguishability of 0.90 and a Purcell factor of 11.3, with the absolute brightness over 4×10^6 s^{-1} for both exciton and bi-exciton emission [188]. Besides entangled photon pairs, higher-level entangled photon emissions with three or four photons were also achieved with semiconductor QDs [189, 190].

To summarise and compare the commonly used techniques for tuning optical properties of QD-based SPEs. The external photonic structures such as PhC cavities, DBR cavities or optical meta-surfaces offer a cavity mode-QD dipole interactions (the physics discussion regarding this can be traced to Fermi's Golden Rule, which is not the focus in this review), which enhances the brightness, quantum efficiency and purity. In the meantime, because of coupling to their intrinsic optical modes, the coherence (e.g. spectral and polarisation) can also be selected. An external electric field by harnessing Stark effect supports an additional degree of freedom to tune the coherence, provided the device is properly designed by considering the exciton charge states, thermal management and breakdown limits. The various architectures of single QD systems with significantly improved optical properties (brightness, efficiency, purity, and indistinguishability) form the basic building blocks to develop other quantum photonic devices (e.g. repeaters and logic gates) and quantum photonic networks.

3.2. Photonic system with $\geqslant$2 QDs

One key challenge that hinders scalability is the lack of coherence between two or more QDs. In other words, it is impossible to prepare two identical QDs with identical electronic states (determined by their morphology, electrostatic background, atomical defects, etc.). To overcome this, several methods have been proposed to match the coherence. Flagg *et al* utilised an open cavity (glued a PZT stage) for tuning the emission spectrum of InAs QD_1 and a DBR cavity for tuning QD_2 (both QDs show a single photon emission purity $g^2(0) < 0.09$). When the spectrally matched, they observed a HOM invisibility <0.5 for parallel polarised photons [191]. Reindl *et al* exploited photon-assisted emission from the GaAs QDs by bringing the emission spectrum from two QDs together. The two-photon interference measurement showed a high visibility (51 $\pm$ 5%). Further enabled the generation of highly indistinguishable (visibility of 71 $\pm$ 9%) entangled photon pairs (fidelity of 90 $\pm$ 2%) [192]. Partel *et al* have fabricated an InGaAs QD inside a p–i–n structure (schematically shown in figure 11(a)). The Stark effect with an external bias allowed them to have a spectral detuning range of 25 meV (figure 11(b)). From the HOM measurement, a clear anti-bunch <0.5 was observed for the parallel polarised photons from two different QDs, with a two-photon interference visibility of 33 $\pm$ 1% (figure 11(c)) [193]. With the same working mechanism, Papon *et al* achieved a two-photon interference visibility of 79 $\pm$ 2% by fabricating two InAs QDs into a PhC waveguide with a p–i–n structure (figure 11(d)) [194]. A non-linear process, so-called quantum frequency conversion (QFC), was also explored to generate coherent photons emitted from two different QDs. As shown in figure 11(e) (and insets), the photon frequencies emitted from two optically pumped QDs display a difference, which can be compensated by a later wave mixing mechanism at each channel. Such a nonlinear process generates two frequency identical photons at 1550 nm, with a two-photon interference visibility of 29 $\pm$ 3% [195]. With the development of high-quality QDs growth, strong coherence with no external detuning was also observed. For example, Dusanowski *et al* have developed two InAs QDs integrated with a GaAs waveguide, within a DBR cavity (figure 11(f)). Each QD is located at one branch of the waveguiding interferometer, exhibiting a purity of $g^2(0) \leqslant 0.035$ measured from the output ports. From the two-photon interference measurement, the raw visibility is 17 $\pm$ 0.7%, and the post-selected visibility of 66% [57]. Similar results are obtained from two remote (20 m) GaAs QDs (figure 11(g)), where a two-photon (parallel polarised photons) visibility of 93 $\pm$ 0.8% was observed from HOM measurement (figure 11(h)). By taking advantage of the two-photon interference, the author established a quantum CNOT gate as shown in figure 11(i), with an overall quantum processing fidelity of 78.24 $\pm$ 7.53% $< F_{\mathrm{proc}} <$ 88.90 $\pm$ 5.34%. With the two remote QDs, the authors demonstrated created entangled states with entanglement fidelity of $F_{\Psi} = (85.02 \pm 0.97)\%$ [196]. Together with entangled photon pairs generation between QDs, the absorption of single photons between different QDs was also studied [197], forming the basis for QD-based quantum networks [198–201].

Although there are very few works investigating the optical properties of a system comprising more than 3 QDs, the 2-QD quantum system have demonstrated great potential for on-chip scalability. With the tunable optical properties demonstrated with variety of techniques, it is promising that quantum photonic networks composed with more than 3 QDs will be developed in the near future.

3.3. Electrically pumped site-controlled QDs

Electrically pumped semiconductor QDs underpin compact SPEs for quantum information networks. Yuan *et al* deterministically fabricated an InAs QD SPE with a p–i–n structure, where the single QD emission was selected by a metal aperture on top of the device (figure 12(a)). The raw photon purity measured by HBT at 2 μA is as low as 0.34 (figure 12(b)), corresponding to a corrected value of <0.14. The photon invisibility from HOM measurement showed 93% under an injection current of 2 μA (figure 12(c)) [202]. Later the research group observed entangled photon-pair emission from a similar device structure, with a two-photon interference measured entanglement fidelity of 82% and a low FSS of 0.4 $\pm$ 0.1 μeV under an injection current density of 31 nA μm^2 [203]. For the entangled photon pair generation, the FSS originates from the

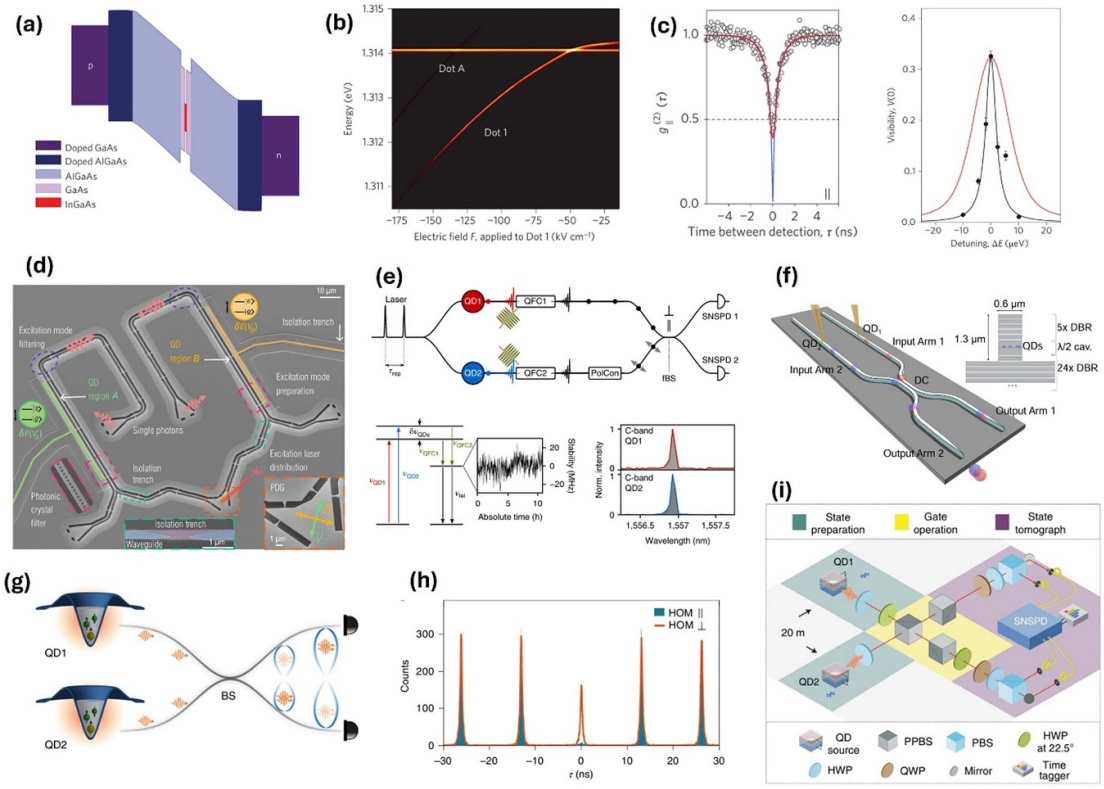

Figure 11. The coherence (indistinguishability) of photons generated from different QDs. (a) Schematic of the energy band structure of an InGaAs QD fabricated into a GaAs p–i–n diode. (b) Under external bias, Dot1 shows a spectral tuning range of 25 meV, which can be matched to the emission from a non-biased DotA. (c) HOM measurements show clear indistinguishability of photons from DotA and Dot1 (left), and photon visibility as a function of detuning energy (right). Reproduced from [193], with permission from Springer Nature. (d) SEM image of two QDs integrated with PhC waveguides for measuring the photon coherence from them. Reproduced from [194]. CC BY 4.0. (e) Schematic and measured coherence from two QD emissions coupled with optical fibres via spectral detuning by two-photon interference. Reproduced from [195], with permission from Springer Nature. (f) On-chip two QDs coherence integrated by a waveguiding interferometer. Reprinted with permission from [57]. Copyright (2023) American Chemical Society. (g) Schematic of measuring photon coherence from two remote QDs with 25 m fibres. (h) The HOM shows raw and corrected visibility of (90.9 ± 0.8)% and (93.0 ± 0.8)% (right). (i) Illustration of a CNOT gate established by two QD SPEs. Reproduced from [196], with permission from Springer Nature.

electro-hole interactions could lift the degeneracy in the bi-exciton cascade emissions, thus causing decoherence of the photon pairs. Chung *et al* investigated a microLED fabricated from site-controlled QDs grown inside pre-pattered inverted pyramids on GaAs substrate [99]. The device structure is shown in figure 12(d), the inverted pyramids were flipped by selectively removing the substrate. Due to the nature of growth, a nanowire on top of the QDs can form a conductive patch for the carrier injection [99, 199, 214]. The authors have fabricated several devices and observed two-photon cascade emission from such QD microLEDs, with the best entanglement fidelity of 0.678 ± 0.023 and small FSS down to 0.2 ± 0.2 μeV (figures 12(e) and (f)) [99]. Electrically injected single QD coupled into a DBR microcavity were also developed [78, 204, 205]. For example, Schneider *et al* have grown site-controlled GaAs QDs on AlAs/GaAs DBR cavity (bottom 25 pairs and top 5 pairs), which were fabricated into electrically injected DBR LED with a diameter of 2.5 μm (figure 12(g)). The devices exhibited a HBT purity of 0.42 (figures 12(h)) and (a) brightness of 1.7×10^5 cps [78]. For a further enhancement of the extraction efficiency, Li *et al* fabricated concentric Brag gratings (bullseye) on the DBR cavity containing a single InAs QD. With external bias, they observed single photon emission with a high purity of 0.03 ± 0.01 and a high brightness of 3.8×10^6 cps (corresponding to an extraction efficiency of 25.44%) [125]. In addition, electrically injected wide bandgap QDs (e.g. InGaN) with emission in visible wavelength range were also realised [53, 110]. For example, Zhang *et al* used top-down method to fabricate site-controlled singe InGaN QD-in-nanowire pin LEDs (figure 12(i)), which showed clear single photon emission ($g^2(0) = 0.42$) under an external bias of 5.7 V (figure 12(j)) [110]. On the platform, the single photon emission will transit from exciton to charged exciton emission, when increasing the applied voltage [116].

From the statistics of the reported results, the optical properties including the purity and invisibility is generally lower than that of the optically pumped ones. This could be resulted from many reasons such as Stark effect by external bias, thermal broadening, electronic noises and so on. Therefore, the next

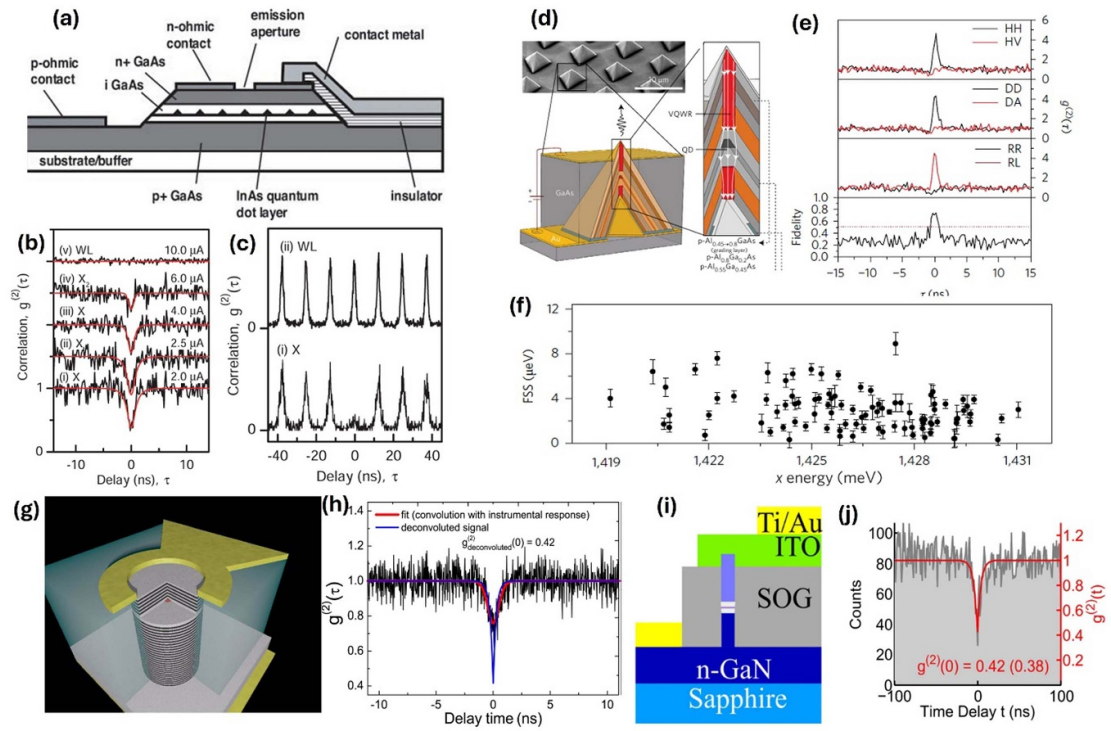

Figure 12. Electrically injected QD-based SPEs fabricated with epitaxial growth and top-down approaches. (a) Schematic of an electrically injected InAs QD SPE, where a metal mask with an aperture allows emission from a single QD to free space. (b) Measured HBT values as a function of cw injected current, with a $g^2(0) = 0.34$ at 2 μA. (c) HBT measurement under pulsed current injection with $g^2(0) = 0.11$. From [202]. © The Authors, some rights reserved; exclusive licensee AAAS. Distributed under a CC BY-NC 4.0 license http://creativecommons.org/licenses/by-nc/4.0/. Reprinted with permission from AAAS. (d) a μLED containing single InAs QD grown on the apex of a GaAs pyramid on a pre-patterned substrate. (e) Two-photon interference measurements under different polarisations from bi-exciton emission, with a best fidelity of 0.73 ± 0.06. (f) Statistics of FSS from various devices showing a minimum value of 0.2 ± 0.2 μeV. Reproduced from [99], with permission from Springer Nature. (g) An electrically injected InAs QD in a DBR p-i-n structure, showing a purity of 0.42 by HBT measurement (h). Reprinted from [78], with the permission of AIP Publishing. (i) Schematic of a GaN LED containing a dot-in-wire structure fabricated by dry etching a single QW. (j) HBT measured $g^2(0) = 0.42$ of the GaN electrical SPE under electrical injection. Reprinted from [110], with the permission of AIP Publishing.

breakthroughs could be the unique designs of QD-based SPEs (e.g. with tunable emission properties) that are immune to such impacts under electrical injection, which may require high crystalline epitaxial layers, potential dielectric passivation, and proper electrical injection methods.

3.4. Optical components simulation and design

Besides the development of semiconductor fabrication, photonic simulation becomes increasingly important for the design of building blocks as well as complex photonic systems. With the advancement and commercialisation of Si photonics, many foundries (e.g. IMEC, GlobalFondries, AIM Photonic etc.) developed each own process design kit (PDKs) assisted by simulations, allowing automatic mass production of the photonic integrated platforms like electronic design automation (EDA) used in electronic integrated circuits (ICs) industry [204, 206, 207, 215]. Similarly, it is also critical for upscaling the QD-based SPEs. For example, the simulation of the modal structure of a photonic structure (e.g. DBR or PhC cavity) integrated with a single QD provides essential information to optimise the coupling efficiency for the desired optical modes [46, 131]. For another example, with the assisted time-domain simulation, the design of concentric Brag grating structures coupled with a single QD enhanced the light-matter interaction, substantially improved the quantum efficiency, purity and indistinguishability [51]. In addition to these progresses, the simulation to design ultra-low loss photonic components (for coherence control and purity filtering) will be the key technical solution for upscaling QD SPEs.

4. Summary and outlook

This review summarises the recent development of site-controlled semiconductor QDs for SPEs, focusing on their fabrication approaches and device performances. Though the site-controlled QDs are still under development, this paper has discussed the visions, challenges and potential solutions in the scalability of such QDs.

Despite the variety of fast-developing quantum materials (such as 2D materials), III–V compound QDs are a promising candidate due to their reliable optical properties, the well-developed fabrication process in the industry, and existing III–V photonic devices on Si (CMOS compatibility). In the meantime, various techniques have been developed for fabricating site-controlled compound QD-based SPEs, summarised as selective-area growth and top-down deterministic fabrication in this paper. It is worth highlighting that each technological route is still under development. Therefore, this paper is not intended to anticipate which technique (or any hybrid technique) will be the eventual solution for scalability. Instead, the recent advancements in this dynamic research area are reviewed to offer a reference from the perspective of engineering SPEs.

Although semiconductor QDs as SPEs have been studied for more than 30 years, most of the research today still focuses on photon emission from an individual QD (including increasing brightness, purity or cascade photon emissions). However, such SPEs require external spatiotemporal multiplex methods to achieve a certain number of photons or q-bits for a quantum photonic system (e.g. 50 photons for Boson sampling to achieve quantum supremacy). Only a limited group have reported coherent photon emission from two (or more) separated QDs [191–196]. Therefore, controlled coherent photon emission from different QDs is critical for on-chip (and long-haul) integrated platforms. This will be the future route to scalable SPEs, which will rely on site-controlled semiconductor QDs. Typical coherence control will involve the modal engineering, spectral filtering and polarisation selection, where the coupled photonic structures (optical cavities, waveguiding devices) and applied electrical/magnetic field could be used as effective manipulation approaches.

In addition to SPEs, it is notable that the light-matter interactions including photon-photonic structures, coupled QDs, and flying q-bit and QDs are intensively studied to develop other quantum photonic components including repeaters, memories, gates etc [208–210]. Besides, on-chip SPDs based on semiconductor and superconducting materials are reported [211, 212]. All these components form the building blocks for realising on-chip (integrated) or long-haul quantum information processing systems, as envisaged in [57] and [213].

Data availability statement

No new data were created or analysed in this study.

Acknowledgment

This work is supported by the SACEME Seedcorn funding (No. YH2024) from Swansea University.

References

[1] Aghaee Rad H *et al* 2025 Scaling and networking a modular photonic quantum computer *Nature* **638** 912–9
[2] Pelucchi E *et al* 2022 The potential and global outlook of integrated photonics for quantum technologies *Nat. Rev. Phys.* **4** 194–208
[3] Zhang G *et al* 2019 An integrated silicon photonic chip platform for continuous-variable quantum key distribution *Nat. Photon.* **13** 839–42
[4] Chang J, Gao J, Esmaeil Zadeh I, Elshaari A W and Zwiller V 2023 Nanowire-based integrated photonics for quantum information and quantum sensing *Nanophotonics* **12** 339–58
[5] Yu Y, Chi Y, Zhai C, Huang J, Gong Q and Wang J 2024 Programmable silicon-photonic quantum simulator based on a linear combination of unitaries *Photon. Res.* **12** 1760–7
[6] Devoret M H and Schoelkopf R J 2013 Superconducting circuits for quantum information: an outlook *Science* **339** 1169–74
[7] Bruzewicz C D, Chiaverini J, McConnell R and Sage J M 2019 Trapped-ion quantum computing: progress and challenges *Appl. Phys. Rev.* **6** 021314
[8] Burkard G, Engel H A and Loss D 2000 Spintronics and quantum dots for quantum computing and quantum communication *Fortschr. Phys.* **48** 965–86
[9] Zhang C, Huang Y F, Liu B H, Li C F and Guo G C 2021 Spontaneous parametric down-conversion sources for multiphoton experiments *Adv. Quantum Technol.* **4** 2000132
[10] Hojo M and Tanaka K 2021 Broadband infrared light source by simultaneous parametric down-conversion *Sci. Rep.* **11** 17986
[11] Meyer-Scott E, Silberhorn C and Migdall A 2020 Single-photon sources: approaching the ideal through multiplexing *Rev. Sci. Instrum.* **91** 041101
[12] Higginbottom D B, Slodička L, Araneda G, Lachman L, Filip R, Hennrich M and Blatt R 2016 Pure single photons from a trapped atom source *New J. Phys.* **18** 093038
[13] Toninelli C *et al* 2021 Single organic molecules for photonic quantum technologies *Nat. Mater.* **20** 1615–28
[14] Brown K R, Chiaverini J, Sage J M and Häffner H 2021 Materials challenges for trapped-ion quantum computers *Nat. Rev. Mater.* **6** 892–905
[15] Abe N, Mitsumori Y, Sadgrove M and Edamatsu K 2017 Dynamically unpolarized single-photon source in diamond with intrinsic randomness *Sci. Rep.* **7** 46722
[16] Pezzagna S, Rogalla D, Wildanger D, Meijer J and Zaitsev A 2011 Creation and nature of optical centres in diamond for single-photon emission—overview and critical remarks *New J. Phys.* **13** 035024

[17] Lohrmann A, Johnson B C, McCallum J C and Castelletto S 2017 A review on single photon sources in silicon carbide *Rep. Prog. Phys.* **80** 034502
[18] Morfa A J, Gibson B C, Karg M, Karle T J, Greentree A D, Mulvaney P and Tomljenovic-Hanic S 2012 Single-photon emission and quantum characterization of zinc oxide defects *Nano Lett.* **12** 949–54
[19] Geng Y, Jena D, Fuchs G D, Zipfel W R and Rana F 2023 Optical dipole structure and orientation of GaN defect single-photon emitters *ACS Photonics* **10** 3723–9
[20] Xue Y *et al* 2020 Single-photon emission from point defects in aluminum nitride films *J. Phys. Chem. Lett.* **11** 2689–94
[21] Lohrmann A, Pezzagna S, Dobrinets I, Spinicelli P, Jacques V, Roch J F and Zaitsev A M 2011 Diamond based light-emitting diode for visible single-photon emission at room temperature *Appl. Phys. Lett.* **99**
[22] Mizuochi N, Makino T, Kato H, Takeuchi D, Ogura M, Okushi H and Yamasaki S 2012 Electrically driven single-photon source at room temperature in diamond *Nat. Photon.* **6** 299–303
[23] Hollenbach M, Klingner N, Jagtap N S, Bischoff L, Fowley C, Kentsch U and Astakhov G V 2022 Wafer-scale nanofabrication of telecom single-photon emitters in silicon *Nat. Commun.* **13** 7683
[24] Pezzagna S and Meijer J 2021 Quantum computer based on color centers in diamond *Appl. Phys. Rev.* **8** 011308
[25] Gazzano O, Michaelis de Vasconcellos S, Arnold C, Nowak A, Galopin E, Sagnes I and Senellart P 2013 Bright solid-state sources of indistinguishable single photons *Nat. Commun.* **4** 1425
[26] Zhou X, Zhai L and Liu J 2023 Epitaxial quantum dots: a semiconductor launchpad for photonic quantum technologies *Photon. Insights* **1** R07
[27] Lodahl P, Mahmoodian S and Stobbe S 2015 Interfacing single photons and single quantum dots with photonic nanostructures *Rev. Mod. Phys.* **87** 347–400
[28] Lin X, Dai X, Pu C, Deng Y, Niu Y, Tong L, Fang W, Jin Y and Peng X 2017 Electrically-driven single-photon sources based on colloidal quantum dots with near-optimal antibunching at room temperature *Nat. Commun.* **8** 1132
[29] Ji Y *et al* 2024 Surface engineering enables efficient $AgBiS_2$ quantum dot solar cells *Nano Lett.* **24** 10418–25
[30] Kagan C R, Bassett L C, Murray C B and Thompson S M 2020 Colloidal quantum dots as platforms for quantum information science *Chem. Rev.* **121** 3186–233
[31] Manikandan A, Chen Y Z, Shen C C, Sher C W, Kuo H C and Chueh Y L 2019 A critical review on two-dimensional quantum dots (2D QDs): from synthesis toward applications in energy and optoelectronics *Prog. Quantum Electron.* **68** 100226
[32] Pal A, Zhang S, Chavan T, Agashiwala K, Yeh C H, Cao W and Banerjee K 2023 Quantum-engineered devices based on 2D materials for next-generation information processing and storage *Adv. Mater.* **35** 2109894
[33] Guo S, Germanis S, Taniguchi T, Watanabe K, Withers F and Luxmoore I J 2023 Electrically driven site-controlled single photon source *ACS Photonics* **10** 2549–55
[34] Gupta S, Wu W, Huang S and Yakobson B I 2023 Single-photon emission from two-dimensional materials, to a brighter future *J. Phys. Chem. Lett.* **14** 3274–84
[35] Ren S, Tan Q and Zhang J 2019 Review on the quantum emitters in two-dimensional materials *J. Semicond.* **40** 071903
[36] Arakawa Y and Holmes M J 2020 Progress in quantum-dot single photon sources for quantum information technologies: a broad spectrum overview *Appl. Phys. Rev.* **7** 021309
[37] Verma V B and Elarde V C 2021 Nanoscale selective area epitaxy: from semiconductor lasers to single-photon sources *Prog. Quantum Electron.* **75** 100305
[38] Gajjela R S R, Sala E M, Heffernan J and Koenraad P M 2022 Control of morphology and substrate etching in InAs/InP droplet epitaxy quantum dots for single and entangled photon emitters *ACS Appl. Nano Mater.* **5** 8070–9
[39] Sala E M, Na Y I, Godsland M, Trapalis A and Heffernan J 2020 InAs/InP quantum dots in etched pits by droplet epitaxy in metalorganic vapor phase epitaxy *Phys. Status Solidi RRL* **14** 2000173
[40] Weisbuch C, Nakamura S, Wu Y R and Speck J S 2020 Disorder effects in nitride semiconductors: impact on fundamental and device properties *Nanophotonics* **10** 3–21
[41] Yang J *et al* 2024 Tunable quantum dots in monolithic Fabry-Perot microcavities for high-performance single-photon sources *Light Sci. Appl.* **13** 33
[42] Yoshie T, Scherer A, Hendrickson J, Khitrova G, Gibbs H M, Rupper G, Ell C, Shchekin O B and Deppe D G 2004 Vacuum Rabi splitting with a single quantum dot in a photonic crystal nanocavity *Nature* **432** 200–3
[43] Chanana A *et al* 2022 Ultra-low loss quantum photonic circuits integrated with single quantum emitters *Nat. Commun.* **13** 7693
[44] Barbiero A, Shooter G, Muller T, Skiba-Szymanska J, Stevenson R M, Goff L E, Ritchie D A and Shields A J 2024 Polarization-selective enhancement of telecom wavelength quantum dot transitions in an elliptical bullseye resonator *Nano Lett.* **24** 2839–45
[45] Stevenson R M, Young R J, See P, Gevaux D G, Cooper K, Atkinson P, Farrer I, Ritchie D A and Shields A J 2006 Magnetic-field-induced reduction of the exciton polarization splitting in InAs quantum dots *Phys. Rev. B* **73** 033306
[46] Winik R, Cogan D, Don Y, Schwartz I, Gantz L, Schmidgall E R, Livneh N, Rapaport R, Buks E and Gershoni D 2017 On-demand source of maximally entangled photon pairs using the biexciton-exciton radiative cascade *Phys. Rev. B* **95** 235435
[47] Reitzenstein S 2012 Semiconductor quantum dot–microcavities for quantum optics in solid state *IEEE J. Sel. Top. Quantum Electron.* **18** 1733–46
[48] Schofield R C *et al* 2024 Bose–Einstein condensation of light in a semiconductor quantum well microcavity *Nat. Photon.* **18** 1083–9
[49] Nomura M, Kumagai N, Iwamoto S, Ota Y and Arakawa Y 2010 Laser oscillation in a strongly coupled single-quantum-dot–nanocavity system *Nat. Phys.* **6** 279–83
[50] Amo A, Lefrère J, Pigeon S, Adrados C, Ciuti C, Carusotto I, Houdré R, Giacobino E and Bramati A 2009 Superfluidity of polaritons in semiconductor microcavities *Nat. Phys.* **5** 805–10
[51] Wang H *et al* 2019 Towards optimal single-photon sources from polarized microcavities *Nat. Photon.* **13** 770–5
[52] Saha P K, Rana K S, Thakur N, Parvez B, Bhat S A, Ganguly S and Saha D 2022 Room temperature single-photon emission from InGaN quantum dot ordered arrays in GaN nanoneedles *Appl. Phys. Lett.* **121** 211101
[53] Deshpande S, Frost T, Hazari A and Bhattacharya P 2014 Electrically pumped single-photon emission at room temperature from a single InGaN/GaN quantum dot *Appl. Phys. Lett.* **105** 141109
[54] Thomson D *et al* 2016 Roadmap on silicon photonics *J. Opt.* **18** 073003
[55] Kaur P, Boes A, Ren G, Nguyen T G, Roelkens G and Mitchell A 2021 Hybrid and heterogeneous photonic integration *APL Photonics* **6** 061102

[56] Gardes F *et al* 2022 A review of capabilities and scope for hybrid integration offered by silicon-nitride-based photonic integrated circuits *Sensors* **22** 4227
[57] Dusanowski Ł, Köck D, Schneider C and Höfling S 2023 On-chip Hong–Ou–Mandel interference from separate quantum dot emitters in an integrated circuit *ACS Photonics* **10** 2941–7
[58] Aharonovich I, Englund D and Toth M 2016 Solid-state single-photon emitters *Nat. Photon.* **10** 631–41
[59] Neergaard-Nielsen J S, Nielsen B M, Takahashi H, Vistnes A I and Polzik E S 2007 High purity bright single photon source *Opt. Express* **15** 7940–9
[60] Matthews J C, Zhou X Q, Cable H, Shadbolt P J, Saunders D J, Durkin G A, Pryde G J and O'Brien J L 2016 Towards practical quantum metrology with photon counting *npj Quantum Inf.* **2** 16023
[61] Meunier M, Eng J J, Mu Z, Chenot S, Brändli V, de Mierry P, Gao W and Zúñiga-Pérez J 2023 Telecom single-photon emitters in GaN operating at room temperature: embedment into bullseye antennas *Nanophotonics* **12** 1405–19
[62] Birowosuto M D, Sumikura H, Matsuo S, Taniyama H, Van Veldhoven P J, Nötzel R and Notomi M 2012 Fast Purcell-enhanced single photon source in 1,550-nm telecom band from a resonant quantum dot-cavity coupling *Sci. Rep.* **2** 321
[63] Farr P, Sidikejiang S, Horenburg P, Bremers H, Rossow U and Hangleiter A 2021 Unity quantum efficiency in III-nitride quantum wells at low temperature: experimental verification by time-resolved photoluminescence *Appl. Phys. Lett.* **119** 011106
[64] Bremer L *et al* 2020 Quantum dot single-photon emission coupled into single-mode fibers with 3D printed micro-objectives *APL Photonics* **5** 106101
[65] Brown R H and Twiss R Q 1956 Correlation between photons in two coherent beams of light *Nature* **177** 27–29
[66] Hong C K, Ou Z Y and Mandel L 1987 Measurement of subpicosecond time intervals between two photons by interference *Phys. Rev. Lett.* **59** 2044
[67] Nakamura Y, Schmidt O G, Jin-Phillipp N Y, Kiravittaya S, Müller C, Eberl K, Gräbeldinger H and Schweizer H 2002 Vertical alignment of laterally ordered InAs and InGaAs quantum dot arrays on patterned (0 0 1) GaAs substrates *J. Cryst. Growth* **242** 339–44
[68] Elarde V C, Yeoh T S, Rangarajan R and Coleman J J 2004 Controlled fabrication of InGaAs quantum dots by selective area epitaxy MOCVD growth *J. Cryst. Growth* **272** 148–53
[69] Huggenberger A, Schneider C, Drescher C, Heckelmann S, Heindel T, Reitzenstein S, Kamp M, Höfling S, Worschech L and Forchel A 2011 Site-controlled In(Ga)As/GaAs quantum dots for integration into optically and electrically operated devices *J. Cryst. Growth* **323** 194–7
[70] Tommila J, Tukiainen A, Viheriälä J, Schramm A, Hakkarainen T, Aho A, Stenberg P, Dumitrescu M and Guina M 2011 Nanoimprint lithography patterned GaAs templates for site-controlled InAs quantum dots *J. Cryst. Growth* **323** 183–6
[71] Choi K, Arita M, Kako S and Arakawa Y 2013 Site-controlled growth of single GaN quantum dots in nanowires by MOCVD *J. Cryst. Growth* **370** 328–31
[72] Ohkouchi S, Nakamura Y, Nakamura H and Asakawa K 2004 Indium nano-dot arrays formed by field-induced deposition with a nano-jet probe for site-controlled InAs/GaAs quantum dots *Thin Solid Films* **464** 233–6
[73] Atkinson P, Ward M B, Bremner S P, Anderson D, Farrow T, Jones G A C, Shields A J and Ritchie D A 2006 Site control of InAs quantum dot nucleation by ex-situ electron-beam lithographic patterning of GaAs substrates *Physica E* **32** 21–24
[74] Atkinson P, Schmidt O G, Bremner S P and Ritchie D A 2008 Formation and ordering of epitaxial quantum dots *C. R. Phys.* **9** 788–803
[75] Ishikawa T, Nishimura T, Kohmoto S and Asakawa K 2000 Site-controlled InAs single quantum-dot structures on GaAs surfaces patterned by *in situ* electron-beam lithography *Appl. Phys. Lett.* **76** 167–9
[76] Li R R, Dapkus P D, Thompson M E, Jeong W G, Harrison C, Chaikin P M, Register R A and Adamson D H 2000 Dense arrays of ordered GaAs nanostructures by selective area growth on substrates patterned by block copolymer lithography *Appl. Phys. Lett.* **76** 1689–91
[77] Hartmann A, Ducommun Y, Loubies L, Leifer K and Kapon E 1998 Structure and photoluminescence of single AlGaAs/GaAs quantum dots grown in inverted tetrahedral pyramids *Appl. Phys. Lett.* **73** 2322–4
[78] Schneider C, Heindel T, Huggenberger A, Niederstrasser T A, Reitzenstein S, Forchel A, Höfling S and Kamp M 2012 Microcavity enhanced single photon emission from an electrically driven site-controlled quantum dot *Appl. Phys. Lett.* **100** 091108
[79] Schneider C, Heindel T, Huggenberger A, Weinmann P, Kistner C, Kamp M, Reitzenstein S, Höfling S and Forchel A 2009 Single photon emission from a site-controlled quantum dot-micropillar cavity system *Appl. Phys. Lett.* **94** 111111
[80] Albert F, Stobbe S, Schneider C, Heindel T, Reitzenstein S, Höfling S, Lodahl P, Worschech L and Forchel A 2010 20100. Quantum efficiency and oscillator strength of site-controlled InAs quantum dots *Appl. Phys. Lett.* **96** 151102
[81] Pérez-Solórzano V, Gröning A, Jetter M, Riemann T and Christen J 2005 Near-red emission from site-controlled pyramidal InGaN quantum dots *Appl. Phys. Lett.* **87** 163121
[82] Choi K, Kako S, Holmes M J, Arita M and Arakawa Y 2013 Strong exciton confinement in site-controlled GaN quantum dots embedded in nanowires *Appl. Phys. Lett.* **103** 171907
[83] Schneider C, Strauß M, Sünner T, Huggenberger A, Wiener D, Reitzenstein S, Kamp M, Höfling S and Forchel A 2008 Lithographic alignment to site-controlled quantum dots for device integration *Appl. Phys. Lett.* **92** 183101
[84] Heinrich J, Huggenberger A, Heindel T, Reitzenstein S, Höfling S, Worschech L and Forchel A 2010 Single photon emission from positioned GaAs/AlGaAs photonic nanowires *Appl. Phys. Lett.* **96** 211117
[85] Tatebayashi J, Ota Y, Ishida S, Nishioka M, Iwamoto S and Arakawa Y 2012 Site-controlled formation of InAs/GaAs quantum-dot-in-nanowires for single photon emitters *Appl. Phys. Lett.* **100** 263101
[86] Mereni L O, Dimastrodonato V, Young R J and Pelucchi E 2009 A site-controlled quantum dot system offering both high uniformity and spectral purity *Appl. Phys. Lett.* **94** 223121
[87] Cho J H, Kim Y M, Lim S H, Yeo H S, Kim S, Gong S H and Cho Y H 2018 Strongly coherent single-photon emission from site-controlled InGaN quantum dots embedded in GaN nanopyramids *ACS Photonics* **5** 439–44
[88] Dalacu D, Mnaymneh K, Lapointe J, Wu X, Poole P J, Bulgarini G, Zwiller V and Reimer M E 2012 Ultraclean emission from InAsP quantum dots in defect-free wurtzite InP nanowires *Nano Lett.* **12** 5919–23
[89] Deng J *et al* 2022 Disk-shaped GaN quantum dots embedded in AlN nanowires for room-temperature single-photon emitters applicable to quantum information technology *ACS Appl. Nano Mater.* **5** 4000–8
[90] Große J, von Helversen M, Koulas-Simos A, Hermann M and Reitzenstein S 2020 Development of site-controlled quantum dot arrays acting as scalable sources of indistinguishable photons *APL Photonics* **5** 096107
[91] Foster A P, Bradley J P, Gardner K, Krysa A B, Royall B, Skolnick M S and Wilson L R 2015 Linearly polarized emission from an embedded quantum dot using nanowire morphology control *Nano Lett.* **15** 1559–63

[92] Haffouz S *et al* 2018 Bright single InAsP quantum dots at telecom wavelengths in position-controlled InP nanowires: the role of the photonic waveguide *Nano Lett.* **18** 3047–52
[93] Hsu C W, Lundskog A, Karlsson K F, Forsberg U, Janzén E and Holtz P O 2011 Single excitons in InGaN quantum dots on GaN pyramid arrays *Nano Lett.* **11** 2415–8
[94] Jemsson T, Machhadani H, Holtz P O and Karlsson K F 2015 Polarized single photon emission and photon bunching from an InGaN quantum dot on a GaN micropyramid *Nanotechnology* **26** 065702
[95] Tachibana K, Someya T, Ishida S and Arakawa Y 2000 Selective growth of InGaN quantum dot structures and their microphotoluminescence at room temperature *Appl. Phys. Lett.* **76** 3212–4
[96] Kim S, Gong S H, Cho J H and Cho Y H 2016 Unidirectional emission of a site-controlled single quantum dot from a pyramidal structure *Nano Lett.* **16** 6117–23
[97] Lundskog A, Hsu C W, Fredrik Karlsson K, Amloy S, Nilsson D, Forsberg U, Olof Holtz P and Janzén E 2014 Direct generation of linearly polarized photon emission with designated orientations from site-controlled InGaN quantum dots *Light Sci. Appl.* **3** e139
[98] Juska G, Dimastrodonato V, Mereni L O, Gocalinska A and Pelucchi E 2013 Towards quantum-dot arrays of entangled photon emitters *Nat. Photon.* **7** 527–31
[99] Chung T H, Juska G, Moroni S T, Pescaglini A, Gocalinska A and Pelucchi E 2016 Selective carrier injection into patterned arrays of pyramidal quantum dots for entangled photon light-emitting diodes *Nat. Photon.* **10** 782–7
[100] Schneider C, Huggenberger A, Gschrey M, Gold P, Rodt S, Forchel A, Reitzenstein S, Höfling S and Kamp M 2012 In (Ga) As/GaAs site-controlled quantum dots with tailored morphology and high optical quality *Phys. Status Solidi a* **209** 2379–86
[101] Strittmatter A *et al* 2012 Site-controlled quantum dot growth on buried oxide stressor layers *Phys. Status Solidi a* **209** 2411–20
[102] Pérez-Solórzano V, Gröning A, Schweizer H and Jetter M 2005 Evidence of different confinement regimes in site-controlled pyramidal InGaN structures *Phys. Status Solidi b* **242** R97–R99
[103] Kwoen J, Watanabe K, Ota Y, Iwamoto S and Arakawa Y 2013 Growth of high-quality InAs quantum dots embedded in GaAs nanowire structures on Si substrates *Phys. Status Solidi c* **10** 1496–9
[104] Mereni L O, Marquardt O, Juska G, Dimastrodonato V, O'Reilly E P and Pelucchi E 2012 Fine-structure splitting in large-pitch pyramidal quantum dots *Phys. Rev. B* **85** 155453
[105] Holmes M, Kako S, Choi K, Arita M and Arakawa Y 2015 Spectral diffusion and its influence on the emission linewidths of site-controlled GaN nanowire quantum dots *Phys. Rev. B* **92** 115447
[106] Reimer M E *et al* 2016 Overcoming power broadening of the quantum dot emission in a pure wurtzite nanowire *Phys. Rev. B* **93** 195316
[107] Schneider C *et al* 2009 Single site-controlled In(Ga)As/GaAs quantum dots: growth, properties and device integration *Nanotechnology* **20** 434012
[108] Felici M, Gallo P, Mohan A, Dwir B, Rudra A and Kapon E 2009 Site-controlled InGaAs quantum dots with tunable emission energy *Small* **5** 938–43
[109] Hou Y, Wang Y and Ai Q 2020 Single photon emission from top-down etched III-nitride quantum dots *Nanotechnology* **31** 13LT01
[110] Zhang L, Teng C H, Ku P C and Deng H 2016 Site-controlled InGaN/GaN single-photon-emitting diode *Appl. Phys. Lett.* **108** 153102
[111] Teng C H, Zhang L, Hill T A, Demory B, Deng H and Ku P C 2015 Elliptical quantum dots as on-demand single photons sources with deterministic polarization states *Appl. Phys. Lett.* **107** 191105
[112] Zhang L, Teng C H, Hill T A, Lee L K, Ku P C and Deng H 2013 Single photon emission from site-controlled InGaN/GaN quantum dots *Appl. Phys. Lett.* **103** 192114
[113] Ellis D J P, Bennett A J, Shields A J, Atkinson P and Ritchie D A 2007 Oxide-apertured microcavity single-photon emitting diode *Appl. Phys. Lett.* **90** 233514
[114] Demory B, Hill T A, Teng C H, Zhang L, Deng H and Ku P C 2015 Plasmonic enhancement of single photon emission from a site-controlled quantum dot *ACS Photonics* **2** 1065–70
[115] Verma V B, Stevens M J, Silverman K L, Dias N L, Garg A, Coleman J J and Mirin R P 2011 Photon antibunching from a single lithographically defined InGaAs/GaAs quantum dot *Opt. Express* **19** 4182–7
[116] Zhang L, Teng C H, Ku P C and Deng H 2016 Charge-tunable indium gallium nitride quantum dots *Phys. Rev. B* **93** 085301
[117] Facsko S, Dekorsy T, Koerdt C, Trappe C, Kurz H, Vogt A and Hartnagel H L 1999 Formation of ordered nanoscale semiconductor dots by ion sputtering *Science* **285** 1551–3
[118] Brunner K, Bockelmann U, Abstreiter G, Walther M, Böhm G, Tränkle G and Weimann G 1992 Photoluminescence from a single GaAs/AlGaAs quantum dot *Phys. Rev. Lett.* **69** 3216
[119] Sartison M, Portalupi S L, Gissibl T, Jetter M, Giessen H and Michler P 2017 Combining *in-situ* lithography with 3D printed solid immersion lenses for single quantum dot spectroscopy *Sci. Rep.* **7** 39916
[120] Kojima T, Kojima K, Asano T and Noda S 2013 Accurate alignment of a photonic crystal nanocavity with an embedded quantum dot based on optical microscopic photoluminescence imaging *Appl. Phys. Lett.* **102** 011110
[121] Liu J, Davanço M I, Sapienza L, Konthasinghe K, De Miranda Cardoso J V, Song J D, Badolato A and Srinivasan K 2017 Cryogenic photoluminescence imaging system for nanoscale positioning of single quantum emitters *Rev. Sci. Instrum.* **88** 023116
[122] Nogues G, Merotto Q, Bachelier G, Hye Lee E and Dong Song J 2013 Fabrication and tuning of plasmonic optical nanoantennas around droplet epitaxy quantum dots by cathodoluminescence *Appl. Phys. Lett.* **102** 231112
[123] Gschrey M, Gericke F, Schüßler A, Schmidt R, Schulze J H, Heindel T, Rodt S, Strittmatter A and Reitzenstein S 2013 In situ electron-beam lithography of deterministic single-quantum-dot mesa-structures using low-temperature cathodoluminescence spectroscopy *Appl. Phys. Lett.* **102** 251113
[124] Liu S *et al* 2017 A deterministic quantum dot micropillar single photon source with> 65% extraction efficiency based on fluorescence imaging method *Sci. Rep.* **7** 13986
[125] Li X *et al* 2023 Bright semiconductor single-photon sources pumped by heterogeneously integrated micropillar lasers with electrical injections *Light Sci. Appl.* **12** 65
[126] Donatini F and Dang L S 2010 A single-step electron beam lithography of buried nanostructures using cathodoluminescence imaging and low temperature *Nanotechnology* **21** 375303
[127] Gschrey M *et al* 2015 Highly indistinguishable photons from deterministic quantum-dot microlenses utilizing three-dimensional in situ electron-beam lithography *Nat. Commun.* **6** 7662
[128] Sapienza L, Davanço M, Badolato A and Srinivasan K 2015 Nanoscale optical positioning of single quantum dots for bright and pure single-photon emission *Nat. Commun.* **6** 7833

[129] Dousse A, Lanco L, Suffczyński J, Semenova E, Miard A, Lemaître A, Sagnes I, Roblin C, Bloch J and Senellart P 2008 Controlled light-matter coupling for a single quantum dot embedded in a pillar microcavity using far-field optical lithography *Phys. Rev. Lett.* **101** 267404
[130] Sapienza L, Liu J, Song J D, Fält S, Wegscheider W, Badolato A and Srinivasan K 2017 Combined atomic force microscopy and photoluminescence imaging to select single InAs/GaAs quantum dots for quantum photonic devices *Sci. Rep.* **71** 6205
[131] Schnauber P *et al* 2018 Deterministic integration of quantum dots into on-chip multimode interference beamsplitters using in situ electron beam lithography *Nano Lett.* **18** 2336–42
[132] Schnauber P, Singh A, Schall J, Park S I, Song J D, Rodt S, Srinivasan K, Reitzenstein S and Davanco M 2019 Indistinguishable photons from deterministically integrated single quantum dots in heterogeneous GaAs/Si_3N_4 quantum photonic circuits *Nano Lett.* **19** 7164–72
[133] Lee K H *et al* 2006 Registration of single quantum dots using cryogenic laser photolithography *Appl. Phys. Lett.* **88** 193106
[134] Hennessy K, Badolato A, Petroff P M and Hu E 2004 Positioning photonic crystal cavities to single InAs quantum dots *Photon. Nanostruct.* **2** 65–72
[135] Kuruma K, Ota Y, Kakuda M, Takamiya D, Iwamoto S and Arakawa Y 2016 Position dependent optical coupling between single quantum dots and photonic crystal nanocavities *Appl. Phys. Lett.* **109** 071110
[136] Hennessy K, Badolato A, Winger M, Gerace D, Atatüre M, Gulde S, Fält S, Hu E L and Imamoğlu A 2007 Quantum nature of a strongly coupled single quantum dot–cavity system *Nature* **445** 896–9
[137] Badolato A, Hennessy K, Atature M, Dreiser J, Hu E, Petroff P M and Imamoglu A 2005 Deterministic coupling of single quantum dots to single nanocavity modes *Science* **308** 1158–61
[138] Gérard J M, Sermage B, Gayral B, Legrand B, Costard E and Thierry-Mieg V 1998 Enhanced spontaneous emission by quantum boxes in a monolithic optical microcavity *Phys. Rev. Lett.* **81** 1110
[139] Springholz G, Holy V, Pinczolits M and Bauer G 1998 Self-organized growth of three-dimensional quantum-dot crystals with fcc-like stacking and a tunable lattice constant *Science* **282** 734–7
[140] Hartmann A, Loubies L, Reinhardt F and Kapon E 1997 Self-limiting growth of quantum dot heterostructures on nonplanar {111} B substrates *Appl. Phys. Lett.* **71** 1314–6
[141] Hartmann A, Loubies L, Reinhardt F, Gustafsson A, Sadeghi A and Kapon E 1998 The evolution of self-ordered quantum dot heterostructures grown on non-planar GaAs 111✓ B substrates *Appl. Surf. Sci.* **123** 329–34
[142] Dalacu D, Mnaymneh K, Sazonova V, Poole P J, Aers G C, Lapointe J, Cheriton R, SpringThorpe A J and Williams R 2010 Deterministic emitter-cavity coupling using a single-site controlled quantum dot *Phys. Rev. B* **82** 033301
[143] Tersoff J, Teichert C and Lagally M G 1996 Self-organization in growth of quantum dot superlattices *Phys. Rev. Lett.* **76** 1675
[144] Xie Q, Madhukar A, Chen P and Kobayashi N P 1995 Vertically self-organized InAs quantum box islands on GaAs (100) *Phys. Rev. Lett.* **75** 2542
[145] Strittmatter A *et al* 2012 Lateral positioning of InGaAs quantum dots using a buried stressor *Appl. Phys. Lett.* **100** 093111
[146] Strauß M, Kaganskiy A, Voigt R, Schnauber P, Schulze J H, Rodt S, Strittmatter A and Reitzenstein S 2017 Resonance fluorescence of a site-controlled quantum dot realized by the buried-stressor growth technique *Appl. Phys. Lett.* **110** 111101
[147] Lundskog A, Hsu C W, Nilsson D, Karlsson K F, Forsberg U, Holtz P O and Janzén E 2013 Controlled growth of hexagonal GaN pyramids by hot-wall MOCVD *J. Cryst. Growth* **363** 287–93
[148] Gong S H, Kim S, Kim J H, Cho J H and Cho Y H 2018 Site-selective, two-photon plasmonic nanofocusing on a single quantum dot for near-room-temperature operation *ACS Photonics* **5** 711–7
[149] Ohkouchi S, Sugimoto Y, Ozaki N, Ishikawa H and Asakawa K 2007 Selective growth of InAs quantum dots using In nano-dot arrays formed by nano-jet probe method *J. Cryst. Growth* **301** 726–30
[150] Zhang W, Shi Z, Huo D, Guo X, Zhang F, Chen L, Wang Q, Zhang B and Peng C 2018 In-situ laser nano-patterning for ordered InAs/GaAs (001) quantum dot growth *Appl. Phys. Lett.* **112** 153108
[151] Wang Y R, Jin C Y, Ho C H, Chen S, Francis H and Hopkinson M 2019 Thermodynamic processes on a semiconductor surface during in-situ multi-beam laser interference patterning *IET Optoelectron.* **13** 7–11
[152] Wang Y R, Olaizola S M, Han I S, Jin C Y and Hopkinson M 2020 Direct patterning of periodic semiconductor nanostructures using single-pulse nanosecond laser interference *Opt. Express* **28** 32529–39
[153] Wang Y R, Han I S, Jin C Y and Hopkinson M 2020 Precise arrays of epitaxial quantum dots nucleated by in situ laser interference for quantum information technology applications *ACS Appl. Nano Mater.* **3** 4739–46
[154] Wang Y R, Han I S, Jin C Y and Hopkinson M 2020 Formation of laterally ordered quantum dot molecules by in situ nanosecond laser interference *Appl. Phys. Lett.* **116** 201901
[155] Thon S M, Rakher M T, Kim H, Gudat J, Irvine W, Petroff P M and Bouwmeester D 2009 Strong coupling through optical positioning of a quantum dot in a photonic crystal cavity *Appl. Phys. Lett.* **94** 111115
[156] Verma V B and Coleman J J 2008 High-density patterned quantum dot arrays fabricated by electron beam lithography and wet chemical etching *Appl. Phys. Lett.* **93** 111117
[157] Verma V B, Reddy U, Dias N L, Bassett K P, Li X and Coleman J J 2010 Patterned quantum dot molecule laser fabricated by electron beam lithography and wet chemical etching *IEEE J. Quantum Electron.* **46** 1827–33
[158] Miyazawa T, Takemoto K, Sakuma Y, Hirose S, Usuki T, Yokoyama N, Takatsu M and Arakawa Y 2005 Single-photon generation in the 1.55-μm optical-fiber band from an InAs/InP quantum dot *Jpn. J. Appl. Phys.* **44** L620
[159] Takemoto K, Takatsu M, Hirose S, Yokoyama N, Sakuma Y, Usuki T, Miyazawa T and Arakawa Y 2007 An optical horn structure for single-photon source using quantum dots at telecommunication wavelength *J. Appl. Phys.* **101** 081720
[160] Androvitsaneas P *et al* 2023 Direct-write projection lithography of quantum dot micropillar single photon sources *Appl. Phys. Lett.* **123** 094001
[161] Lee L K and Ku P C 2012 Fabrication of site-controlled InGaN quantum dots using reactive-ion etching *Phys. Status Solidi c* **9** 609–12
[162] Javadi A *et al* 2015 Single-photon non-linear optics with a quantum dot in a waveguide *Nat. Commun.* **6** 8655
[163] Coles R J, Price D M, Dixon J E, Royall B, Clarke E, Kok P, Skolnick M S, Fox A M and Makhonin M N 2016 Chirality of nanophotonic waveguide with embedded quantum emitter for unidirectional spin transfer *Nat. Commun.* **7** 11183
[164] Siampour H, O'Rourke C, Brash A J, Makhonin M N, Dost R, Hallett D J, Clarke E, Patil P K, Skolnick M S and Fox A M 2023 Observation of large spontaneous emission rate enhancement of quantum dots in a broken-symmetry slow-light waveguide *Npj Quantum Inf.* **9** 15
[165] Chan M L, Tiranov A, Appel M H, Wang Y, Midolo L, Scholz S, Wieck A D, Ludwig A, Sørensen A S and Lodahl P 2023 On-chip spin-photon entanglement based on photon-scattering of a quantum dot *npj Quantum Inf.* **9** 49

[166] Uppu R *et al* 2020 Scalable integrated single-photon source *Sci. Adv.* **6** eabc8268
[167] Liu F *et al* 2018 High Purcell factor generation of indistinguishable on-chip single photons *Nat. Nanotechnol.* **13** 835–40
[168] Carter S G, Sweeney T M, Kim M, Kim C S, Solenov D, Economou S E, Reinecke T L, Yang L, Bracker A S and Gammon D 2013 Quantum control of a spin qubit coupled to a photonic crystal cavity *Nat. Photon.* **7** 329–34
[169] Volz T, Reinhard A, Winger M, Badolato A, Hennessy K J, Hu E L and Imamoğlu A 2012 Ultrafast all-optical switching by single photons *Nat. Photon.* **6** 605–9
[170] Jin C Y, Johne R, Swinkels M Y, Hoang T B, Midolo L, Van Veldhoven P J and Fiore A 2014 Ultrafast non-local control of spontaneous emission *Nat. Nanotechnol.* **9** 886–90
[171] Unsleber S, He Y M, Gerhardt S, Maier S, Lu C Y, Pan J W, Gregersen N, Kamp M, Schneider C and Höfling S 2016 Highly indistinguishable on-demand resonance fluorescence photons from a deterministic quantum dot micropillar device with 74% extraction efficiency *Opt. Express* **24** 8539–46
[172] Nowak A K *et al* 2014 Deterministic and electrically tunable bright single-photon source *Nat. Commun.* **5** 3240
[173] Ginés L *et al* 2022 High extraction efficiency source of photon pairs based on a quantum dot embedded in a broadband micropillar cavity *Phys. Rev. Lett.* **129** 033601
[174] Somaschi N *et al* 2016 Near-optimal single-photon sources in the solid state *Nat. Photon.* **10** 340–5
[175] Muller A, Flagg E B, Bianucci P, Wang X Y, Deppe D G, Ma W, Zhang J, Salamo F G, Xiao M and Shih C K 2007 Resonance fluorescence from a coherently driven semiconductor quantum dot in a cavity *Phys. Rev. Lett.* **99** 187402
[176] Trojak O J, Park S I, Song J D and Sapienza L 2017 Metallic nanorings for broadband, enhanced extraction of light from solid-state emitters *Appl. Phys. Lett.* **111** 021109
[177] Woolf A, Puchtler T, Aharonovich I, Zhu T, Niu N, Wang D, Oliver R and Hu E L 2014 Distinctive signature of indium gallium nitride quantum dot lasing in microdisk cavities *Proc. Natl Acad. Sci.* **111** 14042–6
[178] Davanco M, Liu J, Sapienza L, Zhang C Z, De Miranda Cardoso J V, Verma V, Mirin R, Nam S W, Liu L and Srinivasan K 2017 Heterogeneous integration for on-chip quantum photonic circuits with single quantum dot devices *Nat. Commun.* **8** 889
[179] Wang Y *et al* 2023 Deterministic photon source interfaced with a programmable silicon-nitride integrated circuit *npj Quantum Inf.* **9** 94
[180] Dusanowski Ł, Köck D, Shin E, Kwon S H, Schneider C and Höfling S 2020 Purcell-enhanced and indistinguishable single-photon generation from quantum dots coupled to on-chip integrated ring resonators *Nano Lett.* **20** 6357–63
[181] Zadeh I E, Elshaari A W, Jöns K D, Fognini A, Dalacu D, Poole P J, Reimer M E and Zwiller V 2016 Deterministic integration of single photon sources in silicon based photonic circuits *Nano Lett.* **16** 2289–94
[182] Katsumi R, Ota Y, Osada A, Yamaguchi T, Tajiri T, Kakuda M, Iwamoto S, Akiyama H and Arakawa Y 2019 Quantum-dot single-photon source on a CMOS silicon photonic chip integrated using transfer printing *APL Photonics* **4** 036105
[183] Osada A, Ota Y, Katsumi R, Kakuda M, Iwamoto S and Arakawa Y 2019 Strongly coupled single-quantum-dot–cavity system integrated on a CMOS-processed silicon photonic chip *Phys. Rev. Appl.* **11** 024071
[184] Moroni S T, Varo S, Juska G, Chung T H, Gocalinska A and Pelucchi E 2019 Vanishing biexciton binding energy from stacked, MOVPE grown, site-controlled pyramidal quantum dots for twin photon generation *J. Cryst. Growth* **506** 36–39
[185] Braun T, Unsleber S, Baumann V, Gschrey M, Rodt S, Reitzenstein S, Schneider C, Höfling S and Kamp M 2013 Cascaded emission of linearly polarized single photons from positioned InP/GaInP quantum dots *Appl. Phys. Lett.* **103** 191113
[186] Müller M, Bounouar S, Jöns K D, Glässl M and Michler P 2014 On-demand generation of indistinguishable polarization-entangled photon pairs *Nat. Photon.* **8** 224–8
[187] Liu J *et al* 2019 A solid-state source of strongly entangled photon pairs with high brightness and indistinguishability *Nat. Nanotechnol.* **14** 586–93
[188] Wang H *et al* 2019 On-demand semiconductor source of entangled photons which simultaneously has high fidelity, efficiency, and indistinguishability *Phys. Rev. Lett.* **122** 113602
[189] Arashida Y, Ogawa Y and Minami F 2011 Four-photon cascade from quadexcitons in a single GaAs quantum dot *Phys. Rev. B* **84** 125309
[190] Schmidgall E R, Schwartz I, Gantz L, Cogan D, Raindel S and Gershoni D 2014 Deterministic generation of a quantum-dot-confined triexciton and its radiative decay via three-photon cascade *Phys. Rev. B* **90** 241411
[191] Flagg E B, Muller A, Polyakov S V, Ling A, Migdall A and Solomon G S 2010 Interference of single photons from two separate semiconductor quantum dots *Phys. Rev. Lett.* **104** 137401
[192] Reindl M, Jöns K D, Huber D, Schimpf C, Huo Y, Zwiller V, Rastelli A and Trotta R 2017 Phonon-assisted two-photon interference from remote quantum emitters *Nano Lett.* **17** 4090–5
[193] Patel R B, Bennett A J, Farrer I, Nicoll C A, Ritchie D A and Shields A J 2010 Two-photon interference of the emission from electrically tunable remote quantum dots *Nat. Photon.* **4** 632–5
[194] Papon C, Wang Y, Uppu R, Scholz S, Wieck A D, Ludwig A, Lodahl P and Midolo L 2023 Independent operation of two waveguide-integrated quantum emitters *Phys. Rev. Appl.* **19** L061003
[195] Weber J H, Kambs B, Kettler J, Kern S, Maisch J, Vural H, Jetter M, Portalupi S L, Becher C and Michler P 2019 Two-photon interference in the telecom C-band after frequency conversion of photons from remote quantum emitters *Nat. Nanotechnol.* **14** 23–26
[196] Zhai L, Nguyen G N, Spinnler C, Ritzmann J, Löbl M C, Wieck A D, Ludwig A, Javadi A and Warburton R J 2022 Quantum interference of identical photons from remote GaAs quantum dots *Nat. Nanotechnol.* **17** 829–33
[197] Delteil A, Sun Z, Fält S and Imamoğlu A 2017 Realization of a cascaded quantum system: heralded absorption of a single photon qubit by a single-electron charged quantum dot *Phys. Rev. Lett.* **118** 177401
[198] Lodahl P 2017 Quantum-dot based photonic quantum networks *Quantum Sci. Technol.* **3** 013001
[199] Rota M B, Basset F B, Tedeschi D and Trotta R 2020 Entanglement teleportation with photons from quantum dots: toward a solid-state based quantum network *IEEE J. Sel. Top. Quantum Electron.* **26** 1–16
[200] Yu Y, Liu S, Lee C M, Michler P, Reitzenstein S, Srinivasan K, Waks E and Liu J 2023 Telecom-band quantum dot technologies for long-distance quantum networks *Nat. Nanotechnol.* **18** 1389–400
[201] Li T, Yang G J and Deng F G 2016 Heralded quantum repeater for a quantum communication network based on quantum dots embedded in optical microcavities *Phys. Rev. A* **93** 012302
[202] Yuan Z, Kardynal B E, Stevenson R M, Shields A J, Lobo C J, Cooper K, Beattie N S, Ritchie D A and Pepper M 2002 Electrically driven single-photon source *Science* **295** 102–5
[203] Salter C L, Stevenson R M, Farrer I, Nicoll C A, Ritchie D A and Shields A J 2010 An entangled-light-emitting diode *Nature* **465** 594–7

[204] Unrau W, Quandt D, Schulze J H, Heindel T, Germann T D, Hitzemann O, Strittmatter A, Reitzenstein S, Pohl U W and Bimberg D 2012 Electrically driven single photon source based on a site-controlled quantum dot with self-aligned current injection *Appl. Phys. Lett.* **101** 211119
[205] Sartison M, Seyfferle S, Kolatschek S, Hepp S, Jetter M, Michler P and Portalupi S L 2019 Single-photon light-emitting diodes based on preselected quantum dots using a deterministic lithography technique *Appl. Phys. Lett.* **114** 222101
[206] Siew S Y *et al* 2021 Review of silicon photonics technology and platform development *J. Lightwave Technol.* **39** 4374–89
[207] Bogaerts W and Chrostowski L 2018 Silicon photonics circuit design: methods, tools and challenges *Laser Photon. Rev.* **12** 1700237
[208] Neuwirth J, Basset F B, Rota M B, Roccia E, Schimpf C, Jöns K D, Rastelli A and Trotta R 2021 Quantum dot technology for quantum repeaters: from entangled photon generation toward the integration with quantum memories *Mater. Quantum Technol.* **1** 043001
[209] Thomas S E *et al* 2024 Deterministic storage and retrieval of telecom light from a quantum dot single-photon source interfaced with an atomic quantum memory *Sci. Adv.* **10** eadi7346
[210] Kim H, Bose R, Shen T C, Solomon G S and Waks E 2013 A quantum logic gate between a solid-state quantum bit and a photon *Nat. Photon.* **7** 373–7
[211] Lomonte E, Wolff M A, Beutel F, Ferrari S, Schuck C, Pernice W H and Lenzini F 2021 Single-photon detection and cryogenic reconfigurability in lithium niobate nanophotonic circuits *Nat. Commun.* **12** 6847
[212] Martinez N J, Gehl M, Derose C T, Starbuck A L, Pomerene A T, Lentine A L, Trotter D C and Davids P S 2017 Single photon detection in a waveguide-coupled Ge-on-Si lateral avalanche photodiode *Opt. Express* **25** 16130–9
[213] Lu C Y and Pan J W 2021 Quantum-dot single-photon sources for the quantum internet *Nat. Nanotechnol.* **16** 1294–6
[214] Baier M H, Constantin C, Pelucchi E and Kapon E 2004 Electroluminescence from a single pyramidal quantum dot in a light-emitting diode *Appl. Phys. Lett.* **84** 1967–9
[215] Sun C, Du L and Zhao J 2021 A brief review of design and simulation methodology in silicon photonics *Tsinghua Sci. Technol.* **27** 526–33